Lineaments derived from analysis of linear features mapped from LANDSAT images of the Four Corners Region of the Southwestern United States

Daniel H. Knepper, Jr.

U.S. Geological Survey
Denver, Colorado

Open-File Report 82-849

1982

CONTENTS

ILLUSTRATIONS

Abstract

Linear features are relatively short, distinct, non-cultural linear elements mappable on Landsat multispectral scanner images (MSS). Most linear features are related to local topographic features, such as cliffs, slope breaks, narrow ridges, and stream valley segments that are interpreted as reflecting directed aspects of local geologic structure including faults, zones of fracturing (joints), and the strike of tilted beds.

6,050 linear features were mapped on computer-enhanced Landsat MSS images of 11 Landsat scenes covering an area from the Rio Grande rift zone on the east to the Grand Canyon on the west and from the San Juan Mountains, Colorado, on the north to the Mogollon Rim on the south. Computer-aided statistical analysis of the linear feature data revealed 5 statistically important trend intervals: 1.) N.10W.-N.16E., 2.) N.35-72E., 3.) N.33-59W., 4.) N.74-83W., and 5.) N.89-9-W. and N.89-90E. Subsequent analysis of the distribution of the linear features indicated that only the first three trend intervals are of regional geologic significance. Computer-generated maps of the linear features in each important trend interval were prepared, as well as contour maps showing the relative concentrations of linear features in each trend interval. These maps were then analyzed for patterns suggestive of possible regional tectonic lines.

20 possible tectonic lines, or lineaments, were interpreted from the maps. One lineament is defined by an obvious change in overall linear feature concentrations along a northwest-trending line cutting across northeastern Arizona. Linear features are abundant northeast of the line and relatively scarce to the southwest. The remaining 19 lineaments represent the axes of clusters of parallel linear features elongated in the direction of the linear feature trends. Most of these lineaments mark previously known structural zones controlled by linear features in the Precambrian basement or show newly

recognized relationships to geological and/or geophysical patterns that suggest probable influence by buried basement features. The remaining few lineaments are not strongly correlative with geological or geophysical patterns, but on the basis of existing data they cannot be dismissed as being possible expressions of basement features.

INTRODUCTION

This report summarizes the results of computer analyses of the distribution and preferred orientation characteristics of linear features mapped from computer-enchanced Landsat multispectral scanner (MSS) images of the Four Corners region, Colorado, New Mexico, Utah, and Arizona. Computer-compatible magnetic tapes of 11 Landsat scenes were acquired from the EROS Data Center, Sioux Falls, South Dakota, and digitally processed in the Branch of Petrophysics and Remote Sensing Image Processing Laboratory (Figure 1 and Table 1). Contrast-stretched and edge-enchanced 1:800,000-scale positive transparencies were prepared for each of the 4 bands of Landsat MSS data for each scene (8 images per scene).

Linear features were photogeologically interpreted on the Landsat images, compiled on 1:250,000 topographic base maps, and digitized for computer analysis. Statistical techniques were used to determine the preferred orientation characteristics of the linear feature data and computer graphics were used to prepare maps of the linear features in important azimuthal trend intervals. To facilitate the interpretation of areal distribution patterns, contour maps showing the relative concentration of linear features in the important trend intervals were also prepared. Lineaments formed by boundaries between major concentration domains and by elongated clusters of parallel linear features were then defined and compared to regional geological and geophysical data.

Table 1. Landsat used in mapping the linear features in the Four Corners region. Scene numbers correspond to scene centers shown in Figure 1.

Scene #	Scene ID	Date	Sun Elevation ($_0$)	Sun Azimuth ($_0$)
1	1337-17320	6/25/73	62	111
2	2873-17001	6/13/77	56	102
3	2513-17144	6/18/76	59	102
4	2584-17060	8/18/76	49	125
5	2584-17063	8/28/76	49	123
6	1408-17260	9/04/73	52	130
7	2637-16584	10/20/76	34	144
8	2493-17032	5/29/76	59	108
9	2493-17034	5/29/76	59	106
10	2636-16533	10/19/76	36	143
11	2636-16535	10/19/76	37	142

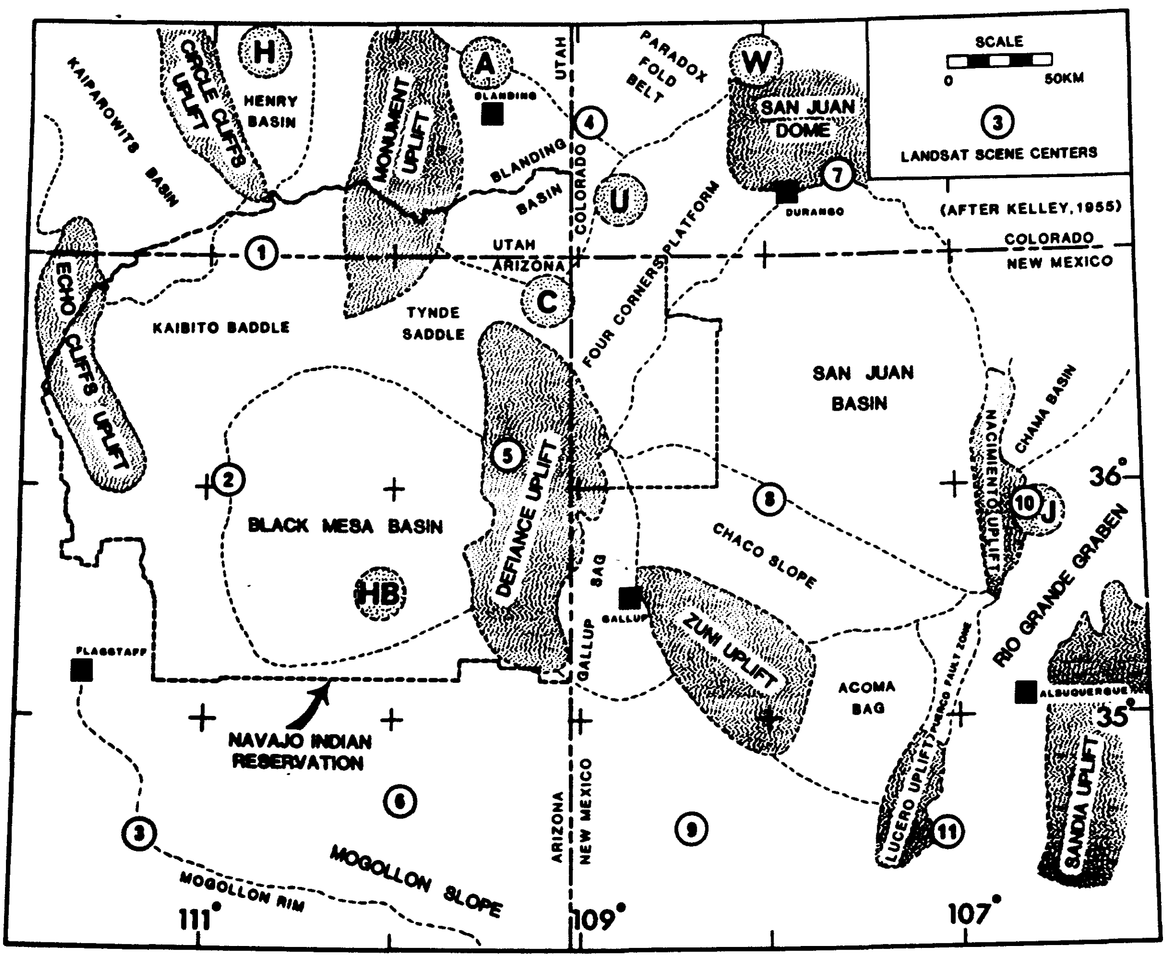

Figure 1. Index map of the Four Corners region showing major tectonic features and centers of Landsat scenes used in this study. Intrusive centers--H,Henry Mountains; A,Abajo Mountains; U,Ute Mountains; W,Wilson Peak; C,Carrizo Mountains; HB,Hopi Buttes; J,Jemez Mountains.

Several investigations have dealt with the mapping and interpretation of linear features and lineaments from Landsat images of portions of the area covered by this study. In northeastern Arizona, Gutman and Heckmann (1977) mapped faults and indistinct structural elements from Landsat images and attempted to correlate these features with known geological features and anomalous patterns in gravity and magnetic data. No systematic analysis of the regional patterns formed by the linear features and lineaments was conducted. Babcock and others (1979) also mapped linear features on Landsat images of northeastern Arizona to test the possibility of using these data as a basis for exploring for fracture-controlled water supplies. Knepper (1978) mapped linear features from Landsat images of the Rio Grande rift zone in north-central New Mexico and discovered possible tectonic zones through statistical analysis of preferred orientation characteristics and analysis of patterns formed by linear feature concentrations. Gableman (J. W. Gableman, unpub. data) studied lineaments and spectral patterns mapped from Landsat images of the Grants uranium belt, New Mexico, to determine whether these data reflect known uranium occurrences and, Zech and Knepper (1979) reported the length and preferred orientation characteristics of linear features mapped from Landsat images of the Gallup-Grants mineral belt. In a paper illustrating the concept of "structural corridors" defined on Landsat lineament maps and regional gravity and magnetic maps, O'Driscoll (1981) identified north-west-trending discontinuities in the pattern of lineament densities displayed on an optically diffused lineament map that includes the northern 75 percent of the Four Corners region.

LANDSAT DATA AND IMAGE PROCESSING

Users can acquire Landsat MSS imagery data from the EROS Data Center, Sioux Falls, South Dakota, in a variety of forms. For this study, the digital data were acquired on 9-track, 1600 BPI computer-compatible magnetic tapes. One tape contains all the digital data numbers (DN) for the four bands of MSS data of a single scene, as well as supplementary information about the data. The four bands of MSS data, identified by NASA as bands 4, 5, 6, and 7, contain measurements of solar radiation reflected from the earth's surface in the wavelength ranges of .5-.6, .6-.7, .7-.8, and .8-1.1 μm, respectively. Bands 4 and 5 correspond to the green and red portions of the visible spectrum; bands 6 and 7 are in the near-infrared.

Processing of the digital MSS data consists of three sets of operations: 1) preparation of the data, 2) computer enhancement, and 3) preparation of hardcopy images. Preparing the MSS data set mainly involves getting the data from the EROS data tape on to a magnetic disk where they are readily available for subsequent computer processing operations. The MSS data on the EROS data tape are contained in four files that represent the image data in four geographic strips of ground coverage needed to produce a full Landsat scene. Within these files, the data for the four MSS bands are interleaved (NASA band interleaved format) such that each tape record contains all the DN values for a single sanline of the image. The four EROS tape files are read into the computer, reformatted, and placed on a large-volume magnetic disk. The four disk files are then concatenated to produce a single, large disk file representing the band interleaved MSS data for the full geographic coverage of the Landsat scene. This large disk file is suitable for input into the computer enhancement programs.

Computer enhancement involves the manipulation of the digital MSS data in order to ultimately produce images that are more easily interpreted. Two types of computer enhancement were used: contrast stretching and edge enhancement. On the EROS data tape, the DN values in bands 4, 5, and 6 are in the range of 0-127, although they usually occupy only a portion of that range: band 7 data are in the DN range of 0-64. In the preparation of black and white images, 256 gray levels are available for displaying the data. By stretching the MSS DN values to occupy the full 256 gray levels, the image contrast between DN values is significantly increased. Contrast stretched images were prepared for each band of MSS data for each of the 11 Landsat scenes.

Edge enhancement is a type of high-pass filter that enhances the high frequency information contained in the MSS data. Figure 2 illustrates the edge enhancement algorithm used in this study. The effect of edge enhancement is to increase the DN contrast at boundaries between groups of dissimilar pixels (picture elements), thereby producing sharper boundaries on black-and-white images. The edge enhanced data are contrast stretched in a manner similar to that described above before images are made on film.

The final step in digital image processing is to prepare high-quality hardcopy images that are suitable for visual interpretation. First, the data need to be corrected for geometric distortions inherent in the MSS data (Condit and Chavez, 1979, p. 11). These distortions are caused by oversampling in the scanline direction (aspect ratio distortion) and the rotation of the earth during a Landsat pass (skew distortion). The geometrically corrected, computer-enhanced data are then used to modulate a light source that exposes black and white film in proportion to the DN values of the processed data, producing film transparencies. The scale of the

EDGE ENHANCEMENT

	N	
W	X	E
	S	

ALGORITHM:

$$\text{ENHANCED DN} = X + \text{ADDBACK FACTOR} \left[4X - (W+E+N+S)\right]$$

ORIGINAL DATA

4	4	4	2	2	2
4	4	4	2	2	2
4	4	4	2	2	2
4	4	4	2	2	2
4	4	4	2	2	2
4	4	4	2	2	2

ENHANCED DATA

4	4	5	1	2	2
4	4	5	1	2	2
4	4	5	1	2	2
4	4	5	1	2	2
4	4	5	1	2	2
4	4	5	1	2	2

$$\text{ENHANCED DN} = 4 + 0.5 \left[16 - (14)\right] = 5$$

Figure 2. Edge enhancement algorithm and an example of how it enhances the linear boundary between 4's and 2's in the original data. The 0.5 addback factor used in the sample calculation of the pixel shown by the dashed line generally produces good results.

transparencies is a function of the playback instrument used to expose the film. The images prepared for this study were made on a Optronics International P-1700 photographic playback system,[1] which allows the full Landsat scene to be recorded on a 10"x10" piece of film at a scale of 1:800,000.

IMAGE INTERPRETATION

The 1:800,000-scale black and white transparencies of the contrast stretched and edge enhanced images of each Landsat scene were used in the mapping of linear features in the Four Corners region. The term "linear feature", as used in this report, refers to distinct, non-cultural linear elements observed in the MSS images. No attempt was made to identify vague or uncertain linear features or to interpret long, discontinuously expressed lineaments. From their appearance on the images and by plotting the mapped linear features on 1:250,000-scale topographic maps, it was determined that most of the linear features are expressions of topographic features such as cliffs, slope breaks, resistant dikes, and stream valley segments. However, numerous linear features were mapped that are expressed on the images as sharp tonal boundaries, but that are not related to topography. These linear features are caused by spectral differences between adjacent rock or soil units or between areas with different vegetation types or densities.

For each individual Landsat scene, linear features were mapped on a separate mylar overlay by successively transferring the overlay to each of the contrast-stretched and edge enhanced images prepared for the scene. Mapping was done on a light table using standard photogeologic interpretation methods. Interpretation continued until no additional linear features could

[1] Trade names used in this paper are for descriptive purposes only and do not constitute endorsement by the U.S. Geological Survey.

be identified; the mapped linear features for each scene were compiled on 1:250,000 topographic maps. This allowed linear features related to cultural features to be excluded from the data set and provided an easy means of resolving the duplicate mapping of linear features in the overlap areas between adjacent Landsat scenes. The compiled linear features were then digitized to produce a digital linear feature data set suitable for analysis by statistical methods.

It should be noted that the Landsat images used in this study were also used to conduct spectral reflectance studies in the Four Corners region, and this necessitated the selection of images having a moderately high solar illumination angle (Table 1). The use of images having a lower solar illumination angle would have allowed additional linear features to be detected and mapped because of increased shadow enhancement; however, the regional patterns displayed in the data probably would not be significantly different.

LINEAR FEATURE ANALYSIS

A total of 6,050 linear features were mapped from the Landsat images of the Four Corners region, producing a complex map that is difficult to analyze by visual inspection alone (Figure 3). Locally, some patterns can be recognized as being of possible geologic importance, but regional relationships are obscure. The objective of linear feature analysis is to dissect the linear feature data into important elements and to display these elements in a manner more conducive to regional geologic analysis. The properties of linear features that can be measured and compared are their length, orientation, and location. Statistical analysis of the linear features according to orientation serves to define regionally important azimuthal trend intervals that may relate to regional geologic or tectonic phenomena. The distribution patterns formed by the linear features in the important azimuthal trend intervals are useful for evaluating the geologic significance of the linear feature data. These patterns can be displayed by using computer techniques to prepare maps of the linear features in the important trend intervals, as well as contour maps showing the relative density or concentration of the linear features within each trend interval.

Strike-Frequency Analysis

The strike-frequency analysis procedure used in this study is a statistical method for helping to define important azimuthal trend intervals within the linear feature data set. The method is described in detail by Sawatzky and Raines (1981) and a brief summary is given here. The strike-frequency analysis computer program counts the number of linear features (frequency) in each of 180 1-degree azimuthal trends and compares these frequencies to the mean frequency of the 180 classes. Some smoothing is accomplished by generating frequency counts that are the average of the initial count plus the adjacent 1-degree intervals. The significance value of any given frequency is based on the probability of that frequency occurring in a data set of known size selected from a uniform population of azimuthal directions. Frequencies near the mean frequency have low significance values, and when the counted frequency equals the mean frequency the significance value is 0. As the frequency deviates from the mean frequency, either positively or negatively, the significance value increases and significant maxima (high frequency) can be defined at significance values selected by the user.

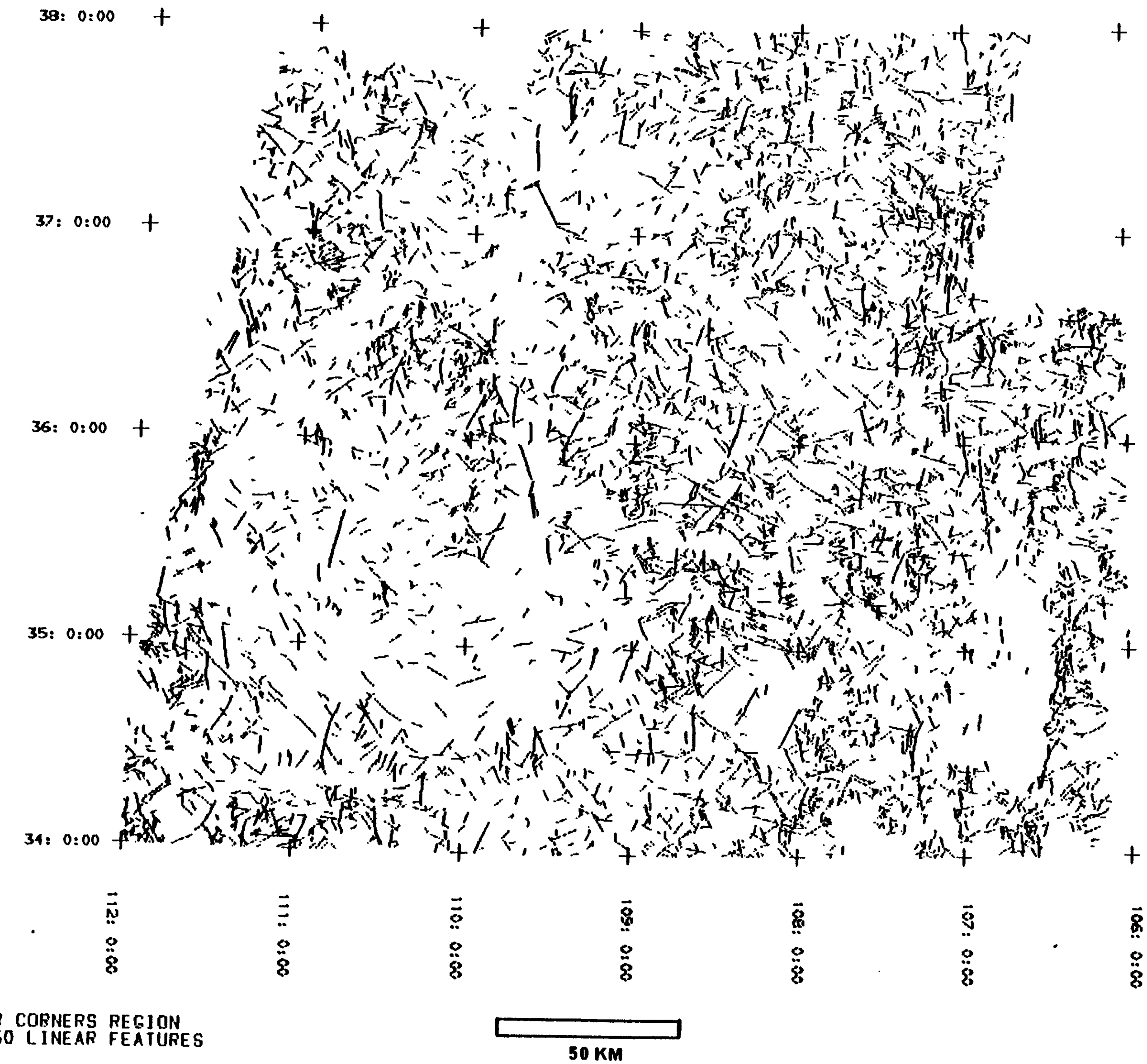

Figure 3. Computer-generated map of digitized linear features mapped in the Four Corners region.

Most of the linear features are short and straight and can be digitized by specifying their end points. However, some linear features are curvilinear and several points along their length need to be digitized to get a good representation. These linear features are composed of segments. Strike frequency analysis can be conducted on either linear features or segments of linear features. If the analysis is conducted on linear features, an average orientation, weighted in proportion to segment lengths, is computed for multi-segment linear features. When the analysis is conducted on segments, each segment of a multi-segment linear feature is treated as an individual, single-segment linear feature. The strike frequency analysis can also be weighted in proportion to the length of the linear feature or segments, thus allowing the longer linear features and segments to more strongly influence the results of the analysis. In length-weighted analyses of linear features, the length-weighting factor of multisegment linear features is the sum of the segment lengths.

Four versions of the strike-frequency analysis were conducted on the linear feature data from the Four Corners region: 1) linear features, 2) length-weighted linear features, 3) segments, and 4) length-weighted segments. The computer output of each analysis consists of three parts: a smoothed strike frequency histogram, a table of azimuth versus frequency for each of the 180 1-degree classes, and a frequency versus significance value curve. Copies of the computer printout for the four analyses are in Appendix A.

The objective of strike frequency analysis is to identify one or more azimuthal trend intervals that appear to be important. The process consists of two steps: 1) identifying the 1-degree intervals that are maxima and minima at a selected significance value and 2) defining clusters of significant 1-degree maxima and minima that form important azimuthal trend intervals. Individual 1-degree maxima and minima can be determined from the computer printout of each analysis by first selecting significance values for maxima and minima from the frequency versus significance value curve and noting the frequencies at which they occur. For maxima, all frequencies equal to or greater than that of the selected significance value will be significant and for minima all frequencies equal to or less than that of the selected significance value will be significant. The significant 1-degree maxima and minima can then be identified on the table of azimuth versus frequency for the analysis. For this study, a simple graphical method was used to identify clusters of 1-degree maxima and minima that appear to form important trend intervals. The 1-degree maxima and minima for each analysis were plotted on four stacked bar graphs each representing 180 degrees of azimuth. Trend intervals were then selected by visual examination of the results of the four analyses.

Results of the strike-frequency analyses are shown in Figure 4. Five trend intervals were selected from the analyses (Table 2). Each of the trend intervals, with the exception of the NS interval, are composed only of 1-degree significant maxima or non-significant frequencies in their respective analyses. The NS interval contains significant 1-degree minima as well, but the pattern of the maxima and minima in this interval is distinctly different than the dominantly minima zones on either sides.

From inspection of the results of the frequency analysis shown in Figure 4, the NS, NE, and NW intervals (Table 2) were further subdivided for geologic analysis. These subdivisions, shown in Table 3, were selected on the basis of the distribution of significant maxima within each larger interval. The subdivided trend intervals proved to be the more useful during geologic interpretation.

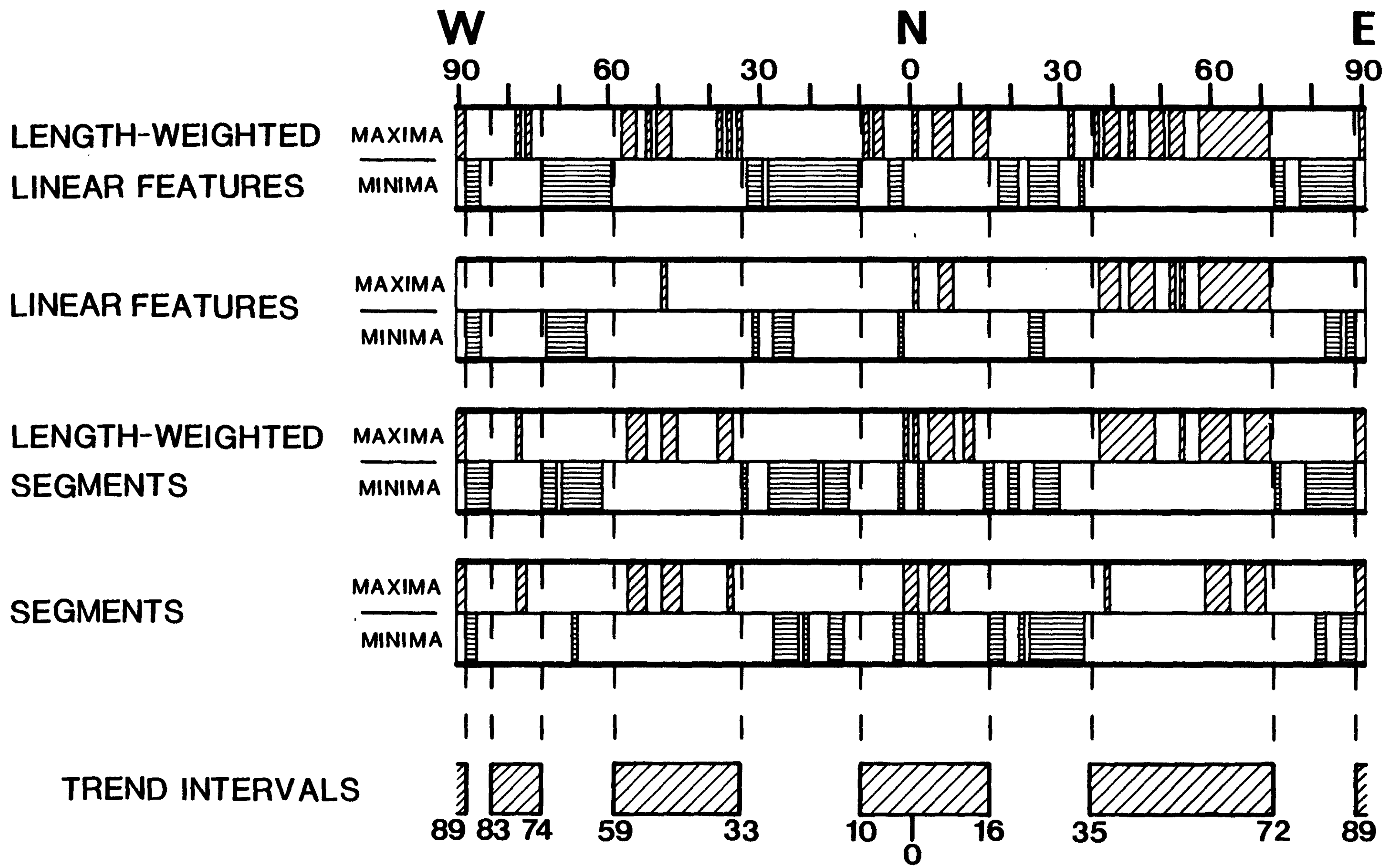

Figure 4. Significant maxima and minima from the four strike frequency analyses, showing the interpreted important trend intervals.

Table 2. Important trend intervals determined by strike-frequency analysis of the linear features data of the Four Corners region.

	Interval Designation	Strike Range	Width (degrees)
1.	NS	N10W-N16E	27
2.	NE	N35-72E	38
3.	NW	N33-59W	27
4.	WNW	N74-83W	10
5.	EW	N89-90W and N89-90E	3

Table 3. Subdivisions of major intervals based on inspection of maxima distribution in the major trend intervals.

Major Interval	Subdivisions	Width (degrees)
N10W-N16E		27
	N0-16E	17
	N0-10W	11
N35-72E		38
	N35-57E	23
N33-59W		27
	N33-43W	11
	N43-59W	15

Trend Interval Maps

Strike-frequency analysis is a method for identifying the prominent trend intervals present in the linear features data, however, it tells little or nothing about the possible geologic importance of these trends in the region. To evaluate the linear feature data in a geologic context, the distribution of the linear features in the important trend intervals must be considered. Regional patterns displayed by the linear features can provide a basis for delineating new geologic information and relationships that may be expressed in the linear feature data.

Using computer graphics, two sets of maps showing the regional distribution of the linear features in the important trend intervals were prepared. The first set (Appendix B) is a series of maps that show the individual linear features in each of the important trend intervals. The second set (Appendix C) is a series of contour maps that show the relative concentrations of the linear features in the important trend intervals. The linear feature concentration maps are particularly useful for delineating regional distribution patterns that are more difficult to visualize on the linear feature trend maps.

GEOLOGIC INTERPRETATION

Geologic interpretation of the linear feature data consists of examining the linear feature and concentration maps for patterns that may represent geologic phenomena. Two types of linear patterns were defined in the Four Corners region: 1) a boundary lineament that divides the area on the basis of relative linear feature concentration and 2) derivative lineaments defined by elongated axes of high linear feature concentration that trend parallel to the linear features that form the concentrations. The interpreted lineaments were compared to regional geologic and geophysical data to determine possible causes of the lineaments and to recognize new geologic relationships. In most cases, the lineaments correspond with geologic or geophysical phenomena, although the direct cause of the lineaments was not determined. In some cases, however, lineaments cannot be strongly associated with known geologic or geophysical data; a clearer definition of these lineaments would probably require substantial additional study, including detailed field work. Figure 5 shows the various lineaments interpreted from the linear data of the Four Corners region.

Domain Boundary Lineament

The most prominent pattern in the linear feature data is a relatively abrupt change in the overall linear feature concentration that occurs along a northwest-trending curvilinear line in the southwestern portion of the area (Fig. 5) This change is apparent on each of the linear feature concentration maps (Appendix C), although the boundary is slightly displaced from trend interval to trend interval; the domain boundary lineament is shown as a zone on Figure 5 that approximately represents the range of boundary locations seen on the various trend interval concentration maps.

The domain boundary lineament marks a regional geomorphic change reflected in the degree of dissection and drainage patterns. Southwest of the lineament is an expanse of relatively undissected plateaus characterized by a parallel drainage pattern formed by northeast-trending tributaries of the Little Colorado River. Because of relatively slight dissection of the plateau surfaces, topopraphically-expressed linear features are few. Northeast of the lineament plateaus and mesas are numerous; however, there are also monoclinal uplifts, and the undulating regional topographic surface shows a relatively high degree of dissection, and drainage patterns in this region are correspondingly much more complex than southwest of the lineament. The

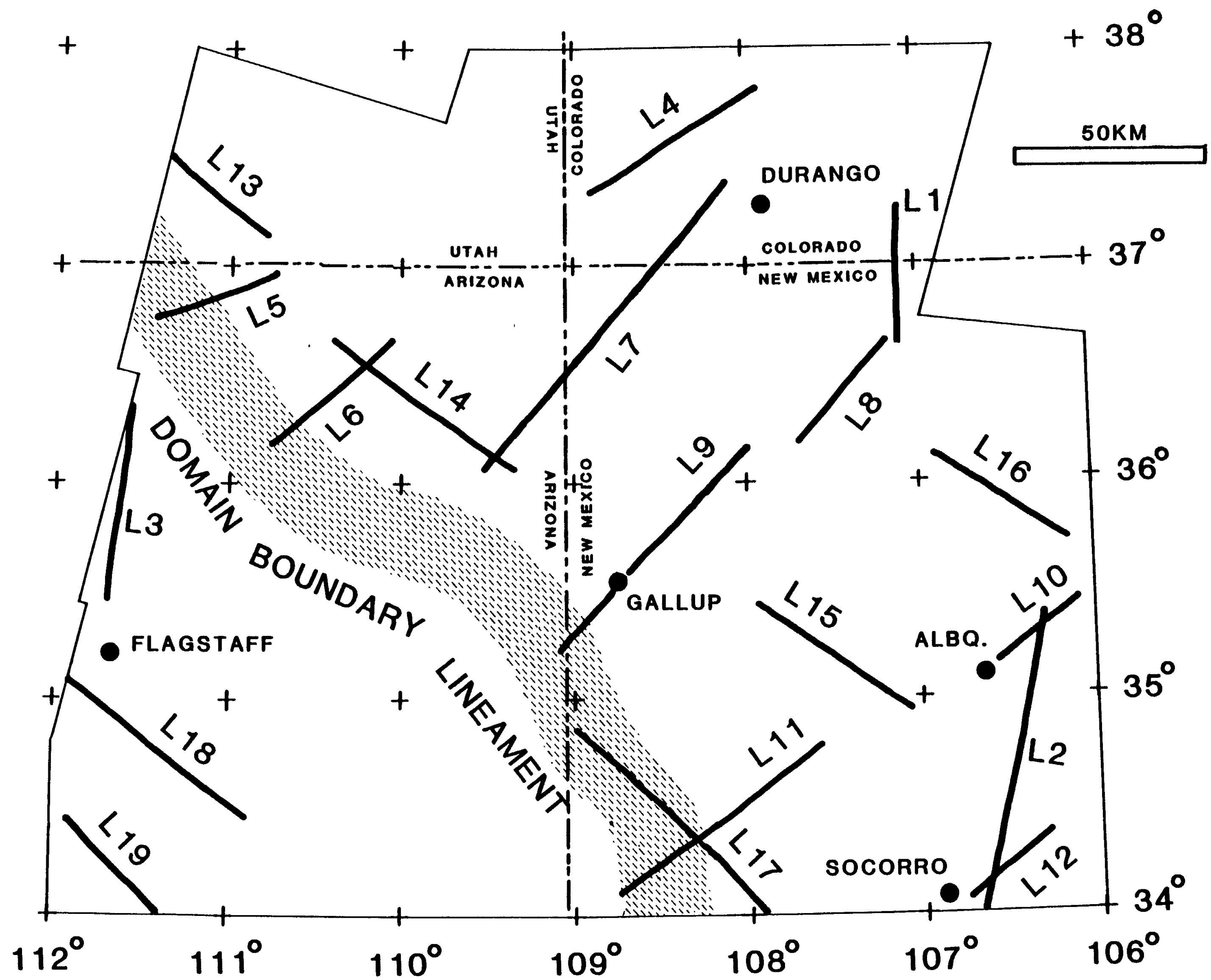

Figure 5. Location of the domain boundary lineament and derivative lineaments in the Four Corners region. Limit of Landsat linear feature data shown by boundary around lineaments.

relatively undissected terrane southwest of the domain boundary lineament extends southwestward to the Mogollon Rim (Fig. 1), which marks the boundary between the Colorado Plateau and the Basin and Range tectonic provinces. Southwest of the Mogollon Rim, Basin and Range structure and topography are responsible for the relatively high linear feature concentrations seen in the southwestern part of the study area.

Other geologic and geophysical data suggest that the geomorphic change represented at the domain boundary lineament does not merely mark a transitory stage in the geomorphic evolotion of the region, but is a geological line that has appeared periodically through time. The establishment of the northwest-trending line is first suggested by the thickness of Devonian strata in the region (Barrs, 1972, p. 94, Fig. 4). The domain boundary lineament lies along the northeastern flank of a conspicuous northwest-trending axis of thin Devonian rocks and appears to delimit the southern extent of the Devonian Ouray Limestone in northeastern Arizona. In Pennsylvanian rocks, the domain boundary lineament coincides with the northwest-trending axis of thin strata that connects the Zuni-Defiance platform with the Piute platform in southern Utah (Mallory, 1972, p. 115, Fig. 4). This arch is parallel to the Pennsylvanian Uncompahgre uplift and appears to mark the southwestern limit of the Paradox basin in Pennsylvanian time. Isopachs of Jurassic rocks generally parallel the trend of the domain boundary lineament except in west-central New Mexico, and the lineament seems to reflect the orientation of the upland area providing sediments northeastward in Jurassic time (Peterson, 1972, p. 180). Within the package of Jurassic rocks in the area, it is interesting that isopachs of Morrison age strata not only have the same general trend as the lineament, but also have the same general shape, and the southwestern edge of these rocks lies only a few kilometers southwest of the lineament (Peterson, 1972, p. 15, Fig. 8). In Pliocene time, interbedded fluvial and lacustrine sediments, mafic lava flows, and rhyolite ash beds of the Bidahochi Formation (Hackman and Olson, 1977) accumulated in a northwest-trending topographic low that parallels and lies partially within the lineament zone in east-central Arizona southeast of Black Mesa. The Hopi Buttes volcanic field lies along the lineament at the northwestern end of the Bidahochi Formation outcrops, and most of the numerous dikes within the volcanic field are oriented to the northwest, parallel to the lineament (Akers and others, 1971).

Geologic structures also seem to reflect the presence of a geological line that corresponds to the domain boundary lineament. Only two major monoclines of the Colorado Plateau (Kelley, 1955; Davis, 1978), the Echo Cliffs and Kaibab monoclines, extend south of the lineament, and these are, in part parallel to it. Three monoclines the Cow Springs, East Defiance, and West Defiance monoclines, terminate at the lineament, and the smaller Red Lake monocline parallels the lineament zone and lies totally within the zone. Likewise, small folds are more numerous northeast of the domain boundary lineament. Near the lineament, most of these folds parallel the lineament zone, and numerous examples occur where northerly trending folds either turn to parallel or terminate as the lineament zone is approached. West of about 111°W. the domain boundary lineament corresponds with a closely-spaced set of northwest-trending faults in the Navajo Sandstone (Cooley and others, 1969) that marks the Morman Ridges fault system of Shoemaker and others, 1978, p. 352.

The domain boundary lineament appears to have a subtle expression on a residual Bouguer gravity map of Arizona prepared by Aiken (1975). The major gravity anomaly in northeastern Arizona is a broad, northeast-trending gravity high with a relatively sharply defined gravity gradient along its southeastern side. Where the domain boundary lineament intersects this gradient, the gravity contours swing abruptly from the northeast trend to a southeast trend paralleling the lineament. On the other hand, regional aeromagnetic data (Sauck and Sumner, 1970) do not appear to reflect the lineament.

Finally, occurrences of uranium/vanadium in eastern Arizona (Keith, 1969) are conspicuously absent from the domain boundary lineament zone, although they are present up to both zone boundaries. This relationship suggests some type of control on uranium/vanadium occurrences by the lineament zone, perhaps on the accumulation of suitable sedimentary host rocks or on the ground-water regime responsible for carrying these elements to their point of deposition.

Derivative Lineaments

Contour maps of the relative concentrations of linear features in each of the important trend intervals defined during statistical analysis were prepared for interpretation. The contour maps were overlaid on their respective linear features maps and a search was made for clusters of parallel and en echelon linear features that form concentration contour patterns elongated in the direction of the trend of the linear features. Where this condition was found, a derivative lineament was visually drawn along the axis of the cluster as depicted on the contour map. Using this technique, 19 derivative lineaments were defined (Fig.5). Appendix D shows the interpretation of the derivative lineaments on the linear feature and linear feature concentration maps of the important trends intervals used in this study.

The reader should keep firmly in mind that the derivative lineaments do not represent knife-edge geological lines that can necessarily be a) seen on a Landsat image or b) easily found in the field. The derivative lineaments are, in effect, statistically defined lines and, consequently, some latitude must be allowed as to their precise meaning and location, particularly during geologic analysis. My interpretation of derivative lineaments is that they represent an approximation of the location of the center of the surface expression of regional linear structural zones of generally variable but undeterminable width. If these zones are controlled by basement structures, then the derivative lineaments represent the approximation of the location of the basement zones at depth. Where the basement rocks are exposed, the derivative lineaments might be expected to be more accurately located than where the basement is overlain by hundreds or thousands of feet of sedimentary and volcanic rocks.

Each of the derivative lineaments was compared to various small-scale geologic and geophysical maps (1:250,000 or smaller) to see what geologic relationships might exist along their trend, These observations are described below. Plate 1 shows the tectonic setting of the derivative lineaments.

North-Trending (L1-3): Derivative lineaments 1, 2, and 3 (Figs. 5 and Plate 1) trend in a general north-south direction and were defined from the linear features map and concentration map of linear features in the N. 0°-16°E. trend interval (Appendix D). Lineament 1 (L1) is south of Pagosa Springs, Colorado, in Archuleta County, Colorado, and Rio Arriba County, New Mexico, in the northeastern corner of the San Juan Basin. It marks the center of a swarm of north-to-north-northeast trending dikes of intermediate to silicic composition (Steven and others, 1974). The dikes form linear ridges that are in contrast to the surrounding topography, making them easy to recognize and map on Landsat images.

Lineament 2 (L2) appears to be defined by linear features that reflect the numerous north-trending faults and fractures associated with the eastern side of the Rio Grande rift zone from northeast of Albuquerque to near

Socorro, New Mexico. The northern part of L2 trends along the uplifted eastern shoulder of the rift, but to the south it more nearly marks the boundary between grabenfill sediments to the west and uplifted Paleozoic and Precambrian rocks to the east.

Lineament 3 (L3) coincides with a long segment of the Oak Creek Canyon fault system of Shoemaker and others (1978, p. 353), north of the San Francisco volcanic field near Flagstaff, Arizona. The linear feature concentration map suggests that L3 may be expressed again south of the volcanic field, but these data are too close to the edge of the data set for a confident interpretation of the contour pattern. Shoemaker and others (1978, p. 358) note that the Oak Creek Canyon fault system (and L3) corresponds to a north-trending magnetic anomaly boundary that is probably controlled by faults with large displacement in the Precambrian basement. However, in a regional sense, the aeromagnetic pattern is not particularly striking (Sauck and Sumner, 1970).

<u>Northeast-Trending (L4-12)</u>: Nine northeast trending derivative lineaments were interpreted from the linear feature and concentration maps of the N.35°-57°E. and N.58°-72°E. trend intervals (Appendix D). Lineament 4 (L4) trends from the Sleeping Ute Mountain igneous center in the southwestern corner of Colorado northeastward to the intrusive center in the San Miguel Mountains near Rico, Colorado. Between these two igneous centers L4 generally corresponds to the House Creek fault and several other faults along the same trend (Haynes and others, 1972). L4 is not dramatically expressed on aeromagnetic data, although it does correspond with the abrupt termination of the southeastern end of a northwest-trending magnetic high (Zietz and Kirby, 1972). In the same area as the apparent magnetic expression, the southwestern half of L4, there is also a conspicuous interruption in the general northwest

trend of gravity contours (Behrendt and Bajwa, 1972). The northeast half of L4 does not seem to be expressed on either aeromagnetic or gravity data.

Lineament 5 (L5) extends from about 14 km northeast of the Echo Cliffs monocline 70 km northeastward across northern Arizona. It approximately marks the northeast-trending boundary between the Kaiparowits Basin and the Kaibito Saddle tectonic divisions of the Colorado Plateau mapped by Kelley (1955, p. 23). L5 also corresponds to a diffuse family of relatively short, northeast-trending faults recognized by Shoemaker and others (1978, p. 344) as the northeastward extension of the Bright Angel fault system that cuts Jurassic rocks from the Navajo Sandstone to the Morrison Formation (Haynes and Hackman, 1978). In aeromagnetic data (Sauck and Sumner, 1970), L5 appears to be expressed by an elongated pattern of high magnetic anomalies and is also on strike with a major northeast-trending zone of basement faulting inferred from magnetic and gravity data by Case and Joesting (1972, Pl. 3) immediately northeast of the northeast end of L5.

Lineament 6 (L6) is parallel to and lies several kilometers southeast of the northeast-trending northwest edge of outcrops of Cretaceous rocks in the central Black Mesa Basin area of northeastern Arizona. The northeast-trending, southeast-facing Organ Rock monocline also parallels this erosional edge of Cretaceous rocks, but lies several kilometers to the northwest of it. It is tempting to relate L6 directly to the Organ Rock monocline; however, inspection of the Landsat linear features that form the concentration pattern defining L6 shows that they are primarily exceptionally linear topographic elements associated with Moenkopi Wash from its intersection with Black Mesa Wash northeastward. This family of linear features is clearly different from those mapped along the Organ Rock monocline. A glance at 1:250,000- and 1:500,000-scale topographic maps of the area reveals that

Moenkopi Wash is an anomalously straight drainage line for about 50 km; other drainages developed on the Cretaceous rocks of the Black Mesa area are also northeast-trending, but they do not maintain linearity for such long distances. No major geologic structures have been documented near Moenkopi Wash. Dips in the Cretaceous rocks are gentle, mostly less than 5°, and minor, broad folds generally trend northwestward across L6. However, minor deflections in the trends of the Cow Springs anticline and the Maloney and Tynde Creek synclines appear to occur where they cross L6. Taken together, the above observations suggest that L6 may mark a fault or fault zone associated with Moenkopi Wash, yet, no faults have been mapped in the vicinity of L6 (Haynes and Hackman, 1978) and gravity and aeromagnetic maps do not reveal evidence for a northeast-trending structure in the area.

Lineament 7 (L7) is the longest of the derivative lineaments, extending 190 km from the Chinle monocline near Canyon De Chelly in northeastern Arizona, across northwestern New Mexico, to the La Plata dome igneous center in southwestern Colorado. Geophysical data indicate that L7 represents a segment of a much longer northeast-trending discontinuity in the Precambrian basement of the Four Corners region (Cordell, 1978, p. 1076). On gravity maps (Aiken, 1975; Suits and Cordell, 1981), L7 lies along a northeast-trending gravity gradient marking the southeastern flank of a broad, northeast-trending gravity high extending from northeastern Arizona to the San Juan volcanic field in southwestern Colorado. This boundary also corresponds to a northeast-trending belt of magnetic anomalies in Arizona (Sauck and Sumner, 1970) that extends from the southwestern end of L7 southwestward through the Hopi Buttes volcanic center to near Phoenix, Arizona. Several other observations suggest that L7 is a real geological line. In the area of the Defiance uplift, intrusive rocks are so common that it is difficult to see any clear alignment of the features related to L7. However, northeast of the Defiance uplift there does appear to be an alignment of intrusive bodies, including northeast-trending minette dikes at Popping Rock, the Shiprock intrusives, minette plugs and northeast-trending dikes near where L7 crosses the Mancos River south of Mesa Verde, and the LaPlata igneous center, from southwest to northeast (O'Sullivan and Beikman, 1963). L7 passes along the Mancos River which marks a geomorphic boundary between the deep, closely-spaced, north to north-northwest oriented canyons of Mesa Verde on the north and the less-numerous canyons of various orientations to the south. Also in this area, L7 passes through the center of the Cretaceous Mesa Verde Basin, which is elongated in a northeast direction along L7 (Haynes, Vogel, and Wyant, 1972). Structurally, the northeastern two-thirds of L7 does not seem to be expressed by mapped structures, although it is parallel to the Hogback monocline about 20 km to the southeast. Where L7 intersects the east flank of the Defiance uplift, however, the bounding Mitten Rock monocline swings abruptly from a north trend to a northeast trend and tends to merge with the Defiance monocline. This results in a conspicuous kink along the east flank of the Defiance uplift. Where L7 crosses the Defiance monocline, the monocline abruptly changes from gentle dips north of L7 to steep dips south of the lineament. At its southwestern end, L7 is parallel to the Tsaile graben about 6 km to the southeast.

Lineament 8 (L8) strikes northeastward across the central San Juan Basin and is entirely within the outcrop area of Tertiary sedimentary rocks. These rocks are more dissected than the surrounding Cretaceous rocks and this may, in part, account for the recognition and mapping of more numerous linear features in the vicinity of L8. However, it is apparent that most of the mapped linear features in this area are oriented in a northeast direction.

There are no folds or faults mapped in the vicinity of L8 (Manley and Scott, 1978) with which to make comparisons of structural orientations. But L8 does mark the axis of a northeast-trending prong of high gravity that protrudes northeastward across the center of the San Juan Basin (Suits and Cordell, 1981) suggesting that there may be a northeast-trending feature in the Precambrian basement that has influenced the development of northeast-trending linear features in the Tertiary sediments.

Lineament 9 (L9) extends northeastward from the southern end of the East Defiance monocline on the New Mexico-Arizona border, across the northwest tip of the Zuni uplift, to a point about 10 km north of Chaco Canyon. L9 marks the southward termination of the East Defiance monocline and the northward termination of the Nutria monocline. This is the type of criterion used by Davis (1978) to infer the presence of major fracture zones in the Precambrian basement of the Colorado Plateau. An aeromagnetic map of the San Juan Basin prepared by the U.S. Geological Survey (1982) shows that L9 trends along the southeastern flank of a northeast-trending ridge of high magnetic intensity that may reflect a highly magnetic intrusive body at depth. The strong northeastward elongation of the magnetic pattern is suggestive of structural control, probably in the Precambrian basement. At the surface, L8 passes through an area in which 2 relatively long northeast-trending linear features were mapped on the Landsat images. One of the linear features is along Pipeline Valley and is particularly long because it passes northeastward across a drainage divide and continues northeastward along Pinetree Canyon as well. The second long linear feature is along Hard Ground Canyon immediately west of Pipeline Valley. The length and straightness of these linear features strongly suggests the presence of faults, but none are shown on published maps of the area. Pipeline Valley is particularly suspect because of the differing nature of the geomorphic character of the terrane on opposite sides of the valley. L8 also marks the northwest end of the Gallup-Grants uranium belt (Melvin, 1976).

Lineament 10 (L10) cuts northeastward across the north end of the Sandia Mountains east of Albuquerque, New Mexico. It passes south of where the eastern boundary fault of the Rio Grande graben, the Rincon fault, swings northeastward and splays into four faults, and north of the northeast-trending Tijeras fault zone. The Landsat linear features forming the concentration pattern that defines L10 include linear features reflecting both of these structural zones; however, most of the linear features appear to be reflecting the numerous northeast-trending faults that occur in the intervening area, such as the Forest, Perlas del Polvo, and Seco faults and the north end of the Barro fault (Kelley and Northrop, 1975). The change from the north trend to the northeast trend of the eastern margin of the Rio Grande graben at the north end of the Sandia Mountains is dramatically displayed in the change in orientation of the steep gravity gradient that works the edge of the graben (Suits and Cordell, 1981). L10 lies along the top (south) edge of this gravity gradient.

Lineament 11 (L11) follows a band of mountainous terrain in west-central New Mexico separating the Quaternary basalt surface of the North Plains on the north from the Quaternary alluvial deposits of the Plains of San Augustine on the south. There appears to be a relatively high concentration of linear features in this area because the alluvium and youthful basalts are not fractured or existing fractures have not been erosionally enhanced to the point of being recognizable on Landsat images; however, the linear features present show a strong preferred orientation in a northeastern direction. The southwest end of L11 corresponds with the northeast end of a northeast-trending zone of faults that can be traced southwestward into eastern Arizona. L11 appears to express a northeastward continuation of this zone of fracturing, although no faults have been mapped. There is no recognizable expression of L11 on available gravity maps.

Lineament 12 (L12) is a relatively short derivative lineament at the southeastern corner of the study area east of Socorro, New Mexico. It approximately marks the path of the Morenci lineament, a major tectonic zone that extends southwestward well into Arizona. The lineament has had a significant influence on the tectonic and magmatic history of the Socorro region. West of Socorro, the Morenci lineament is a shear zone that separates domains of fault blocks that have been tilted and step faulted in opposite directions (Chapin and others, 1978, p. 115). East of Socorro, the lineament appears to be expressed by numerous northeast-trending Tertiary dikes exposed to the vicinity of Canyon Cueva and short, northeast-trending faults a few kilometers east of Socorro (Machette, 1978).

Northwest Trending (L13-19): Seven northwest-trending derivative lineaments were interpreted from the linear feature and concentration maps of the N.33-43W. and N.43-59W. trend intervals (Appendix D). Lineament 13 (L13) marks the northeastern border of the Kaiparowits Plateau, and is the only derivative lineament in Utah. The northeastern edge of the Kaiparowits Plateau is the long erosional scarp of Straight Cliffs, where the resistant capping sandstone units of the Cretaceous Straight Cliffs Sandstone are exposed (Hackman and Wyant, 1973). L13 does not correspond with a known regional structural feature and minor folds in the area show no relationship to the lineament. However, the length and linearity of the Straight Cliffs is certainly suggestive of some type of structural control. The southern two-thirds of L13 does correspond with the straight northeast boundary of a northwest-trending

Bouguer gravity low (Cook and others, 1975). In addition, L13 is a segment of the Zuni lineament of Kelley (1960) and Kelley and Clinton (1960), which was believed to be the most important structure-controlling lineament on the Colorado Plateau.

Lineament 14 (L14) also follows the trend of the Zuni lineament (Kelley, 1955; Kelley and Clinton,1960). The northwestern two-thirds of the L14 trends along the band of Cretaceous Yale Point Sandstone, Mancos Shale, Dakota Sandstone, Wepo Formation, and Toreva Formation outcrops at the northeastern edge of Black Mesa (Haynes and Hackman, 1978). To the southeast, L14 strikes off of Black Mesa, cutting across formational contacts until its termination in the vicinity of the Tsaile graben south of Canyon de Chelly. Along this segment, L14 cuts across structure contours on the base of the Dakota Sandstone at a high angle and no minor structures have been mapped that parallel L14 (O'Sullivan and Beikman, 1963). Along the edge of Black Mesa, however, L14 parallels the northwest-trending Rim syncline until this fold dies out: then it trends parallel to the structure contours on the base of the Dakota Sandstone until its northwest termination at the north-trending Organ Rock monocline near Marsh Pass. Along the northwestern one-thrid of L14, there are numerous north- to northeast-trending minor folds in the Jurassic Morrison Formation northeast of L14 that end abruptly at L14. In the Cretaceous rocks southwest of this portion of L14, minor folds are absent and the strata dip gently to the southwest (Haynes and Hackman, 1978). Several Tertiary minette dikes parallel L14, but they lie 8-12 km northeast of the lineament (Haynes and Hackman, 1978; O'Sullivan and Beikman, 1963). There is no strong or sharp expression of L14 on aeromagnetic data. However, southwest of L14 anomalies tend to be elongated to the north or northeast, whereas northeast of L14 they tend to be oriented in a northwest direction (Sauck and

Sumner, 1970). On gravity data (Aiken, 1975), L14 corresponds to the axis of a shallow northwest-trending gravity depression that is transverse to the major northeast-trending regional gravity high in northeastern Arizona. The northeast-trending gravity contours that define the gravity gradient along the southeast edge of the regional gravity high swing abruptly to the southeast where they are intersected by L14, suggesting that L14 does mark some type of discontinuity in the basement rocks.

Lineament 15 (L15) trends northwestward from near South Garcia in Valencia County, New Mexico, across the Mount Taylor volcanic center, to Mesa Redonda about 10 km west-northwest of Ambrosia Lake, New Mexico. This marks a large segment of the Grants mineral belt, which is characterized by large uranium deposits in the Jurassic rocks on the north flank of the Zuni uplift (Melvin, 1976). The derivative lineament also coincides with the northeastern extent of gypsum-dolomite facies in Permian eolian sandstones and red beds of Leonardian age and marks a northwest-trending axis of relatively thick Leonardian (Rascoe and Barrs, 1972, p. 153, Fig. 7). Structurally, the southeast end of L15 marks the tectonic boundary between the Rio Puerco fault zone on the north and the Lucero uplift on the south (Kelley and Clinton, 1960; Callender and Zilinski, 1976, p. 53, Fig. 1). However, there are few northwest-striking faults along the trend of L15 and, indeed, L15 is transverse to the northeast structural grain in the Rio Puerco fault zone and the Lucero uplift.

Lineament 16 (L16) begins at the east side of Caja del Rio Plateau about 15 km west of Santa Fe, New Mexico, and trends northwesterly across the center of the Vallez caldera to the Nacimiento fault along the west flank of San Pedro Mountain. Northwest of the Vallez caldera there are several northwest-trending structures that are parallel to L16 and are within a few kilometers of it (Manley and Scott, 1978). Southeast of the caldera, there are northwest-trending faults along Canon de Los Frijoles and Alamo Canyon that lie near L16 (Smith and others 1970). In general, though, existing geologic mapping does not depict any obvious structural zone corresponding to L16. Geophysical data, however, suggest quite the opposite. On gravity and aeromagnetic maps the northerly trend of the western margin of the Rio Grande south of L16 turns abruptly to the northwest following L16 for several kilometers before turning back to a northerly trend (Cordell, 1976). Gravity data also show that L16 marks the northern end of a well-defined, narrow, north-trending gravity high associated with the Nacimiento uplift. Steep, north-trending gravity gradients on both sides of the gravity high abruptly turn northeastward when they intersect L16, and the gradient on the west side also decreases markedly in steepness. If L16 is projected southeastward to the eastern margin of the Rio Grande graben, it intersects at the point where the margin changes from a northeast trend along the north end of the Sandia Mountains to a north trend along the base of the Sandgre de Cristo Mountains. Projected to the northwest, L16 marks the northwest-trending oil and gas field in the San Juan Basin. Patterns on regional gravity maps (Cordell and others, 1978; Cook and others 1975) suggest that L16 may be a segment of a gravity lineament that extends as much as 350 km southeast of L16 and northwestward perhaps as far as the Glen Canyon area on southeastern Utah.

Lineaments 17 trends northwestward across volcanic terrain from the Plains of San Augustine in west-central New Mexico to near the New Mexico/Arizona border. The northern two-thirds of L17 is subparallel to and falls within the boundary domain lineament described earlier, but, in general, geologic evidence for a structural zone along the trend of L17 is scant. L17 generally crosscuts regional topographic features, although there is some local parallelism. A few kilometers north of L17 there are several northwest-trending dikes and the north end of L17 is near a northwest-trending fault that extends from near Atargue Lake to near Ajo Caliente. On gravity data (Suits and Cordell, 1981), the southeastern one-half of L17 lies along a northwest-trending ridge of high gravity and the northwestern one-half seems to mark the southern end of a northeast-trending gravity high and parallel low extending southwestward from the Zuni uplift.

Lineament 18 extends northwestward from Chevelon Canyon about 8 km upstream from Chevelon Canyon Lake in the southeast corner of Coconino County, Arizona, across the Mogollon Plateau to Sycamore Creek at it intersection with Volunteer Canyon about 30 km southeast of Flagstaff, Arizona. The southeastern one-third of L18 occurs in Permian sedimentary strata, whereas the remainder is in Tertiary and Quaternary basalts (Wilson and others, 1969). There are a few minor folds in the Permian strata that have the same general trend as L18, and several faults with the same trend as L18 have been mapped in the basalts. At its northwest end, L18 matches up with the southeastern end of the northwest-trending Cataract Creek fault system mapped by Shoemaker and others (1978). The number and length of the linear features mapped from the Landsat images in the area of L18 certainly suggests that the Cataract Creek system continues to the southeast along L18, although it may be dominated by fractures, rather than faults. L18 appears to correspond with the southwestern edge of a belt of northwest-trending aeromagnetic highs (Sauck and Sumner, 1970), but no expression of L18 was seen on gravity data (Aiken, 1975).

Lineament 19 (L19) is in central Arizona about 75 km south of L18. It trends northwestward from the Tonto Basin near Pine Butte, across the Mazatzal Mountains to the Black Hills about 2 km south-southwest of Squaw Peak. The southeastern two-thirds of L19 traverses Precambrian rocks with major faults oriented north-northeast to northeast. The northwestern one-third of L19 traverses Tertiary and Quaternary basaltic rocks with dominant faulting oriented north-northwest to northwest. In general, the evidence for a structural zone along the trend of L19 is not strong. However, if L19 is projected northwestward, it marks the trend of numerous northwest-trending faults in the Black Hills and near Jerome, Arizona, that connect to the Chino Valley fault system of Shoemaker and others (1978). L19 may not represent a southeastern extension of the Chino Valley fault system, but it might reflect a belt of northwest-trending fractures related to it. Aeromagnetic anomalies in the vicinity of L19 are generally oriented northwestward, but L19 does not seem to be singly expressed (Sauck and Sumner), 1970). There are no gravity anomaly patterns corresponding to L19 (Aiken, 1975).

SUMMARY

As the term is used in this study, "linear features" are relatively short, distinct, non-cultural linear elements mappable on Landsat MSS images. In this study, as is generally the case, most of the linear features represent linear topographic features, such as cliffs, slope breaks, narrow ridges, and stream valley segments that are interpreted as reflecting directed aspects of local geologic structure, including faults, zones of fracturing, and the strike of tilted beds. Because of spatial and spectral resolution limitations of the Landsat system, as well as the failure of many geologic structures to be adequately expressed at the earth's surface, many of the geologic structures in a local area may not be recognized on Landsat MSS images. However, mapping of linear features on MSS images provides a sample of the directed geologic structure present.

Landsat MSS images provide a means of acquiring a sample of geologic structures over large areas rapidly and relatively inexpensively. While these data may be insufficient for detailed structural studies of local areas, they are useful for looking for regional relationships indicative of large, often subtly expressed, tectonic features. The analysis techniques used in this study were designed expressly for this purpose.

Computer-enhanced MSS images of eleven Landsat scenes covering the Four Corners region were prepared and used to photographically map 6,050 linear features. Many known faults or segments of known faults were mapped as linear features, however, the number of linear features is many times greater that the number of known faults. This indicates that most linear features represent some other type of geologic structure; I believe that most linear features are controlled by jointing in the rocks exposed at the surface.

The linear features map prepared for the Four Corners region is much too complex to analyze visually for regional geologic relationships. Consequently, computer techniques were used to break the data into important parts and to analyze these parts. The preferred orientation characteristics of the data set were determined by statistical methods and regionally important intervals were selected from the results of statistical analysis. To evaluate the spatial distribution characteristics of linear features in important trend intervals, computer-generated maps of the linear features in each important trend interval were prepared, as well as contour maps of the relative concentrations of linear features in each important trend interval. These maps were then visually analyzed for linear patterns that might reflect tectonic lines.

Twenty possible tectonic lines, or lineaments, were interpreted during the study. One lineament, the domain boundary lineament, is a northwest-trending curvilinear zone that separates overall high linear feature concentration to the northeast from relatively low linear feature concentration to the southeast. The domain boundary lineament appears to mark a geological line that has periodically appeared beginning at least by late Paleozoic time. Of particular interest is the paucity of uranium/vanadium occurrences within the lineament zone, while reported occurrences are relatively numerous on either side of the lineament zone and up to the zone boundaries.

The remaining 19 lineaments are termed derivative lineaments to emphasize that they are not lineaments directly observable on the Landsat images as individual linear features. Rather, they are lines marking the axis of clusters of linears features elongated in the same direction as the linear features that form the clusters, visually interpreted from the trend interval concentration and linear features maps. The reason for mapping derivative lineaments involves the simple concept that elongated clusters of linear features, presumably representing belts of directed geologic structures of which most are fractures, may reflect major tectonic lines. Indeed, several of the derivative lineaments correspond with known fault zones for which evidence of control by the Precambrian basement is very strong. Several other derivative lineaments are not expressed at the surface by known structural zones, but they do mark lines of curious geological associations and/or geophysical features that are suggestive of buried basement features. The remaining few derivative lineaments do not have strong geological or geophysical associations, yet they cannot be dismissed as possible reflections of buried basement phenomena at this time.

REFERENCES

Aiken, C. L. V., 1975, Residual Bouguer gravity anomaly map of Arizona: Laboratory of Geophysics, University of Arizona, Tucson, Arizona, scale 1,000,000.

Akers, J. P., Shorty, J. C., and Stevens, P. R., 1971, Hydrogeology of the Cenozoic igneous rocks, Navajo and Hopi Indian Reservations, New Mexico and Utah: U.S. Geological Survey Prof. Paper 521-D, 18 p.

Babcock, Elizabeth, Briggs, Phillip, Decook, Kenneth, Ethridge, Loch, Foster, Kennith, Glass, Charles, and Schowengerdt, Robert, 1979, Geologic applications of Landsat images in northeastern Arizona to the location of water supplies for municipal and industrial uses: Final report, Office Water Research and Technology, U.S. Department of Interior, Washington, D.C., 92 p.

Barrs, D. L., 1972, Devonian system, in Geologic Atlas of the Rocky Mountain Region: Rocky Mtn. Assoc. Geologists, Denver, p. 90-99.

Behrendt, J. C., and Bajwa, L. Y., 1972, Bouguer gravity map of Colorado: U.S. Geol. Survey Open-File Rept., scale 1:500,000.

Callender, J. F., and Zilinski, R. E., Jr., 1976, Kinematics of Tertiary and Quaternary deformation along the eastern edge of the Lucero uplift, central New Mexico, in Woodward, L. A. and Northrop, S. A., eds., Tectonics and Mineral Resources of Southwestern North America: New Mexico Geol. Soc. Spec, Pub. No. 6, p. 53-61.

Case, J. E., and Joesting, H. R., 1972, Regional geophysical investigations in the central Colorado Plateau: U.S. Geol. Survey Prof. Paper 736, 31 p.

Chapin, C. E., Chamberlin, R. M., Osburn, G. R., White, D. W., and Sanford, A. R., 1978, Exploration framework of the Socorro geothermal area, New Mexico: New Mexico Geol. Soc. Spec. Pub. 7, p. 115-129.

Condit, C. D., and Chavez, P. S., Jr., 1979, Basic concepts of computerized digital image processing for geologists: U.S. Geol. Survey Bull. 1462, 16 p.

Cook, K. L., Montgomery, J. R., Smith, J. T., and Gray, E. F., 1975, Simple Bonguer gravity anomaly map of Utah: Utah Geological and Mineral Survey, Dept. of Natural Resources, Map 37, scale 1:1,000,000.

Cooley, M. E., Harshbarger, J. W., Akers, J. P., and Hardt, W. F., 1969, Regional hydrogeology of the Navajo and Hopi Indian Reservations: U.S. Geol. Survey Prof. Paper 521-A, 61 p.

Cordell, Lindrith, 1976, Aeromagnetic and gravity studies of the Rio Grande graben in New Mexico between Belen and Pilar, in Woodward, L. A. and Northrop, E. E., eds., Tectonics and Mineral Resources of Southwestern North America: New Mexico Geol. Soc. Spec. Pub. No. 6, p. 62-70.

________,1978, Regional geophysical setting of the Rio Grande rift Geol. Soc. America Bull., v. 89, p. 1073-1090.

Dane, G. H., and Bachman, G. O., 1965, Geologic map of New Mexico: U.S. Geological Survey, scale 1:5,000,000.

Davis, G. H., 1978, Monocline fold pattern of the Colorado Plateau, in Matthews, Vincent, III, ed., Laramide folding associated with basement block faulting in the western United States: Geol. Soc. America Mem. 151, p. 215-233.

Gutman, S. I., and Heckman, G. A., 1977, An integration of Landsat and geophysical data in northeastern Arizona: GS Laboratories, Report of Investigations, U.S. Geol. Survey contract 94599, 47 p.

Hackman, R. J., and Olson, A. B., 1977, Geology, structure, and uranium deposits of the Gallup 1° x 2° quadrangle, New Mexico and Arizona: U.S. Geol. Survey Map I-981, scale 1:250,000.

Hackman, R. J., and Wyant, D. G., 1973, Geology, structure, and uranium deposits of the Escalante quadrangle, Utah: U.S. Geol. Survey Miscellaneous Investigations Map I-744, scale 1:250,000.

Haynes, D. D., and Hackman, R. J., 1978, Geology, structure, and uranium deposits of the Marble Canyon 1° x 2° quadrangle, Arizona: U.S. Geol. Survey Miscellaneous Investigations Map I-1003, scale 1:250,000.

Haynes, D. D., Vogel, J. D., and Wyant, D. G., 1972, Geology, structure, and uranium deposits of the Cortez quadrangle, Colorado and Utah: U.S. Geol. Survey Miscellaneous Investigations Map I-629, scale 1:250,000.

Hintze, L. F., 1980, Geologic map of Utah: Utah Geological and Mineral Survey, scale 1:500,000.

Keith, S. B., 1969, Map of known metallic mineral occurrences (excluding base and precious metals) in Arizona: Arizona Bureau of Mines, University of Arizona, Tucson, scale: 1:1,000,000.

Kelley, V. C., 1955, Regional tectonics of the Colorado Plateau and relationship to the origin and distribution of uranium: Univ. of New Mexico Publications in Geology, No. 5, 120 p.

_________, 1978, Features of the rift margin north of the Sandia uplift, in Hawley, J. W., compiler, Guidebook to Rio Grande Rift in New Mexico and Colorado: New Mexico Bur. Mines and Mineral Resources Circ. 163, p. 159-169.

Kelley, V. C., and Clinton, N. J., 1960, Fracture systems and tectonic elements of the Colorado Plateau: Univ. of New Mexico Publications in Geology, No. 6, 104 p.

Kelley, V. C., and Northrop, S. E., 1975, Geology and Sandia Mountains and vicinity, New Mexico: New Mexico Bur. Mines and Mineral Resources Mem. 29, 136 p.

Knepper, D. H., Jr., 1978, Analysis of linear features, Rio Grande rift zone, central New Mexico (abs)., in Conference Proceedings, 1978 International Symposium on the Rio Grande Rift, Santa Fe, New Mexico: Los Alamos Scientific Laboratory Report LA-7487-C, Los Alamos, New Mexico, p. 48-49.

Machette, M. N., 1978, Preliminary geologic map of the Socorro 1° x 2° quadrangle, central New Mexico: U.S. Geol. Survey Open-File Report 78-607, scale 1:250,000.

Mallory, W. W., 1972, Regional synthesis of the Pennsylvanian System, in Geologic Atlas of the Rocky Mountain Region: Rocky Mtn. Assoc. of Geologists, Denver, p. 111-127.

Manley, Kim, and Scott, G. R., 1978, Preliminary geologic map of the Aztec 1° x 2° quadrangle, northwestern New Mexico and southern Colorado: U.S. Geol. Survey Open-File Rept. 78-466, scale 1:250,000.

Melvin, J. W., 1976, Systematic distribution of large uranium deposits in the Grants uranium region, New Mexico, in Woodward, L. A., and Northrop, S. A., eds., Tectonics and Mineral Resources of Southwestern North America: New Mexico Geol. Soc. Spec. Pub. 6, p. 144-150.

O'Driscoll, E. S. T., 1981, Structural corridors in Landsat lineament interpretation: Mineral Deposits, v. 16, p. 85-101.

O'Sullivan, R. B., and Beikman, H. M., 1963, Geology, structure, and uranium deposits of the Shiprock quadrangle, New Mexico and Arizona: U.S. Geol. Survey Miscellaneous Geologic Investigations Map I-345, scale 1:250,000.

Peterson, J. A., 1972, Jurassic System, in Geologic Atlas of the Rocky Mountain Region: Rocky Mtn. Assoc. of Geologists, Denver, p. 177-189.

Rascoe, Bailey, Jr., and Barrs, D. L., 1972, Permian System, in Geologic Atlas of the Rocky Mountain Region: Rocky Mtn. Assoc. of Geologists, Denver, p. 143-165

Sauck, W. A., and Sumner, J. S., 1970, Residual aeromagnetic map of Arizona: Department of Geosciences, University of Arizona, Tucson, scale 1:1,000,000.

Sawatzky, D. L., and Raines, G. L., 1981, Geologic uses of linear feature maps from small-scale imagery: Proceedings of Third International Conference on Basement Tectonics, p. 91-100.

Shoemaker, E. M., Squires, R. L., and Abrams, M. J., 1978, Bright Angel and Mesa Butte fault systems of northern Arizona, in Cenozoic Tectonics and Regional Geophysics of the Western Cordillera: Geol. Soc. America Mem. 152, p. 341-367.

Smith, R. L., Bailey, R. A., and Ross, C. S., 1970, Geologic map of the Jemez Mountains, New Mexico: U.S. Geol. Survey Miscellaneous Investigations Map I-571, scale 1:125,000.

Steven, T. A., Lipman, P. W., Hail, W. J., Jr., Barker, Fred, and Luedke, R. G., 1974, Geologic map of the Durango quadrangle, southwestern Colorado: U.S. Geol. Survey Miscellaneous Investigations Map I-764, scale 1:250,000.

Suits, V. J., and Cordell, Lindrith, 1981, Bouguer gravity map of the San Juan Basin region, Colorado, Arizona, and New Mexico: U.S. Geol. Survey Open-File Rept. 81-657, scale 1:500,000.

Tweto, Ogden, 1979, Geologic map of Colorado: U.S. Geol. Survey Map, scale 1:500,000.

U.S. Geological Survey, 1982, Aeromagnetic map of northeastern Arizona and northwestern New Mexico: U.S. Geol. Survey Open-File Report 80-614, scale 1:500,000.

Wilson, E. D., Moore, R. T., and Cooper, J. R., 1969, Geologic map of Arizona: Tucson Arizona Bur. Mines, scale 1:500,000.

Woodward, L. A., Kaufman, W. H., and Anderson, J. B., 1972, Nacimiento fault and related structures, northern New Mexico: Geol. Soc. America Bull., v. 83, p. 2383-2396.

Zech, R. S., and Knepper, D. H., Jr., 1979, Landsat linear features data of the Gallup-Grants uranium district, New Mexico: U.S. Geol. Survey Open-File Rept. 79-1507, 35 p.

Zietz, Isidore, and Kirby, J. R., 1972, Aeromagnetic map of Colorado: U.S. Geol. Survey Geophysical Investigations Map GP-836, scale 1:500,000.

APPENDIX A

Computer Printout of Strike Frequency Analyses

EMPIRICAL STRIKE FREQUENCY ANALYSIS.

FOUR CORNERS WEIGHTED LINEAR FEATURES

10 LEVELS OF FREQUENCY AT 66 PER LEVEL.

PERCENT AZIMUTH FOR SMOOTHING = 1.67

NO. OF DATA = 27012

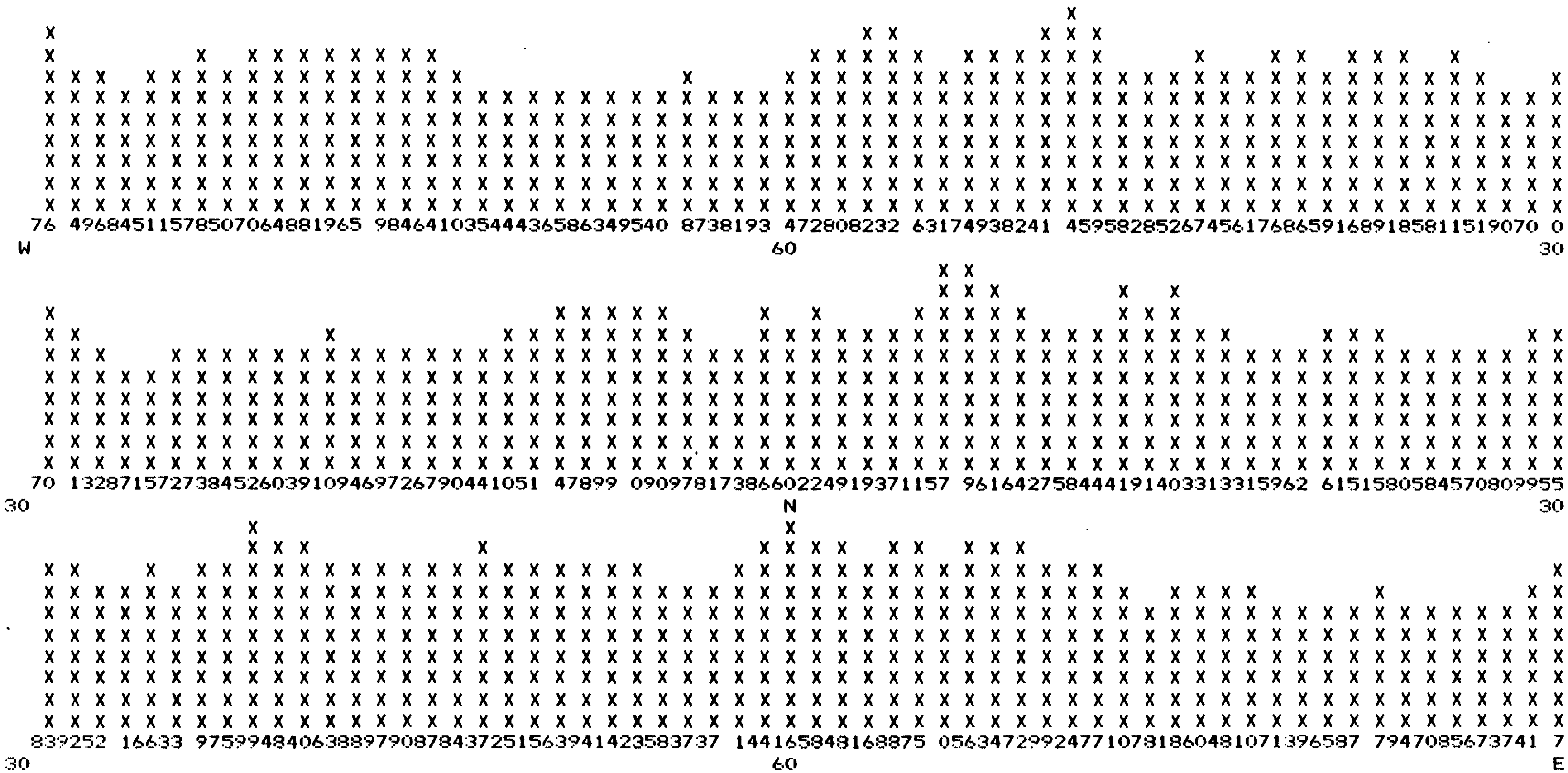

TABLE OF AZIMUTH VS FREQUENCY FOR PRECEDING STRIKE FREQUENCY PLOT

AZIM	BRNG	FREQ	AZIM	BRNG	FREQ	AZIM	BRNG	FREQ	AZIM	BRNG	FREQ
271	-89	576	316	-44	467	1	1	522	46	46	487
272	-88	404	317	-43	445	2	2	449	47	47	484
273	-87	396	318	-42	461	3	3	419	48	48	537
274	-86	384	319	-41	476	4	4	437	49	49	525
275	-85	451	320	-40	486	5	5	511	50	50	515
276	-84	415	321	-39	459	6	6	657	51	51	463
277	-83	478	322	-38	516	7	7	609	52	52	494
278	-82	450	323	-37	489	8	8	561	53	53	514
279	-81	470	324	-36	518	9	9	464	54	54	523
280	-80	464	325	-35	458	10	10	427	55	55	458
281	-79	488	326	-34	511	11	11	458	56	56	437
282	-78	519	327	-33	451	12	12	444	57	57	437
283	-77	465	328	-32	390	13	13	541	58	58	501
284	-76	509	329	-31	370	14	14	491	59	59	544
285	-75	484	330	-30	400	15	15	540	60	60	616
286	-74	464	331	-29	470	16	16	433	61	61	558
287	-73	410	332	-28	401	17	17	413	62	62	548
288	-72	335	333	-27	332	18	18	331	63	63	516
289	-71	344	334	-26	287	19	19	359	64	64	588
290	-70	343	335	-25	315	20	20	362	65	65	575
291	-69	365	336	-24	372	21	21	406	66	66	500
292	-68	386	337	-23	373	22	22	415	67	67	556
293	-67	334	338	-22	384	23	23	415	68	68	534
294	-66	395	339	-21	352	24	24	380	69	69	572
295	-65	340	340	-20	360	25	25	358	70	70	499
296	-64	408	341	-19	339	26	26	345	71	71	524
297	-63	373	342	-18	410	27	27	370	72	72	477
298	-62	381	343	-17	394	28	28	380	73	73	410
299	-61	393	344	-16	369	29	29	399	74	74	378
300	-60	404	345	-15	372	30	30	455	75	75	418
301	-59	472	346	-14	367	31	31	483	76	76	460
302	-58	480	347	-13	390	32	32	492	77	77	448
303	-57	582	348	-12	344	33	33	452	78	78	410
304	-56	532	349	-11	410	34	34	401	79	79	371
305	-55	506	350	-10	451	35	35	466	80	80	339
306	-54	431	351	-9	504	36	36	433	81	81	365
307	-53	474	352	-8	478	37	37	509	82	82	387
308	-52	493	353	-7	499	38	38	475	83	83	407
309	-51	482	354	-6	500	39	39	599	84	84	394
310	-50	541	355	-5	490	40	40	548	85	85	370
311	-49	604	356	-4	397	41	41	540	86	86	385
312	-48	559	357	-3	381	42	42	463	87	87	367
313	-47	458	358	-2	373	43	43	488	88	88	337
314	-46	428	359	-1	486	44	44	497	89	89	441
315	-45	452	360	0	460	45	45	490	90	90	507

FOUR CORNERS WEIGHTED LINEAR FEATURES

FREQUENCY PROBABILITY DATA

NO. OF DATA = 27012 EVENT PROB. = 0.017 PROB. LIMIT = 0.970

FREQUENCY MEAN = 450.2

EMP. FREQ.	REL. FREQ.	FREQ. PROB.	SIGNIF VALUE
411	2.0	0.003	93.6
412	2.0	0.004	92.9
413	2.0	0.004	92.1
414	2.0	0.004	91.2
415	2.0	0.005	90.3
416	2.0	0.005	89.3
417	2.0	0.006	88.2
418	2.0	0.006	87.0
419	2.1	0.006	85.7
420	2.1	0.007	84.4
421	2.1	0.007	82.9
422	2.1	0.008	81.4
423	2.1	0.008	79.7
424	2.1	0.009	78.0
425	2.1	0.009	76.1
426	2.1	0.010	74.2
427	2.1	0.010	72.1
428	2.1	0.011	69.9
429	2.1	0.012	67.6
430	2.1	0.012	65.3
431	2.1	0.013	62.8
432	2.1	0.013	60.2
433	2.1	0.014	57.5
434	2.1	0.014	54.7
435	2.1	0.015	51.8
436	2.1	0.015	48.8
437	2.1	0.016	45.7
438	2.1	0.016	42.5
439	2.1	0.017	39.3
440	2.1	0.017	35.9
441	2.1	0.017	32.5
442	2.1	0.018	29.1
443	2.1	0.018	25.6
444	2.1	0.018	22.0
445	2.1	0.018	18.4
446	2.2	0.019	14.7
447	2.2	0.019	11.1
448	2.2	0.019	7.4
449	2.2	0.019	3.7
450	2.2	0.019	0.0
451	2.2	0.019	0.0
452	2.2	0.019	3.8
453	2.2	0.019	7.6
454	2.2	0.018	11.4
455	2.2	0.018	15.2
456	2.2	0.018	18.9
457	2.2	0.018	22.5
458	2.2	0.017	26.1
459	2.2	0.017	29.7
460	2.2	0.017	[illegible]

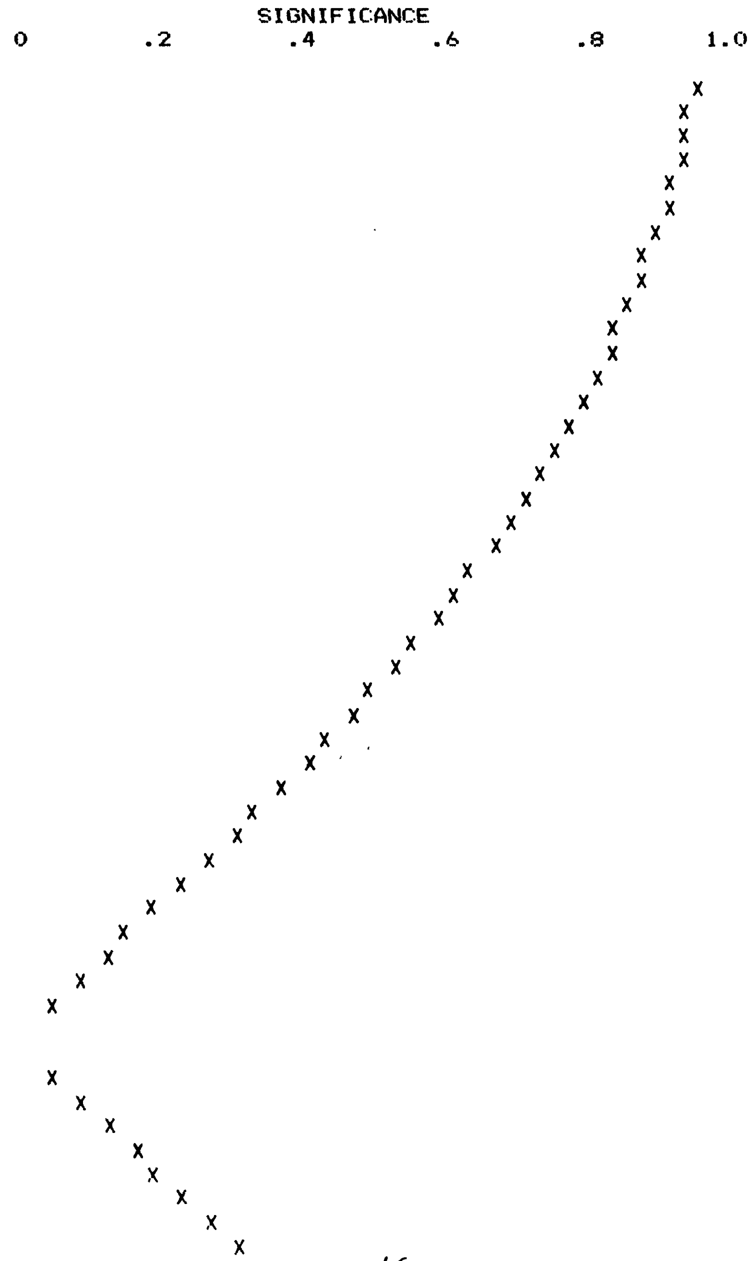

462	2.2	0.016	39.9	
463	2.2	0.015	43.1	
464	2.2	0.015	46.3	
465	2.2	0.015	49.3	
466	2.2	0.014	52.3	
467	2.2	0.014	55.2	
468	2.2	0.013	57.9	
469	2.2	0.013	60.6	
470	2.2	0.012	63.1	
471	2.2	0.011	65.5	
472	2.2	0.011	67.9	
473	2.3	0.010	70.1	
474	2.3	0.010	72.2	
475	2.3	0.009	74.2	
476	2.3	0.009	76.1	
477	2.3	0.008	77.9	
478	2.3	0.008	79.6	
479	2.3	0.007	81.2	
480	2.3	0.007	82.7	
481	2.3	0.006	84.2	
482	2.3	0.006	85.5	
483	2.3	0.006	86.7	
484	2.3	0.005	87.9	
485	2.3	0.005	88.9	
486	2.3	0.005	89.9	
487	2.3	0.004	90.8	
488	2.3	0.004	91.7	
489	2.3	0.004	92.5	
490	2.3	0.003	93.2	
491	2.3	0.003	93.9	

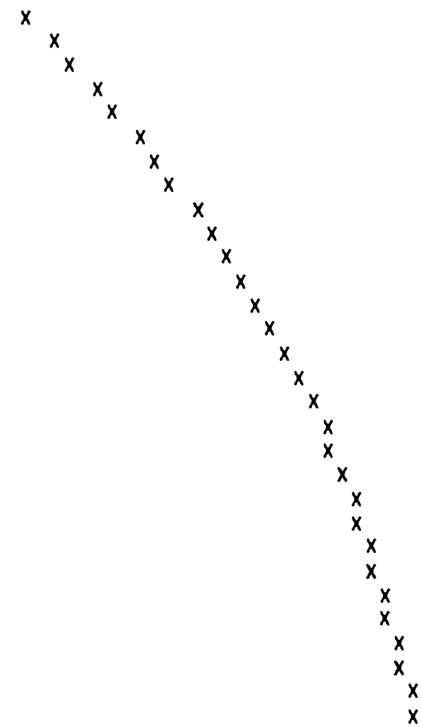

EMPIRICAL STRIKE FREQUENCY ANALYSIS.

FOUR CORNERS LINEAR FEATURES

10 LEVELS OF FREQUENCY AT 15 PER LEVEL.

PERCENT AZIMUTH FOR SMOOTHING = 1.67

NO. OF DATA = 6050

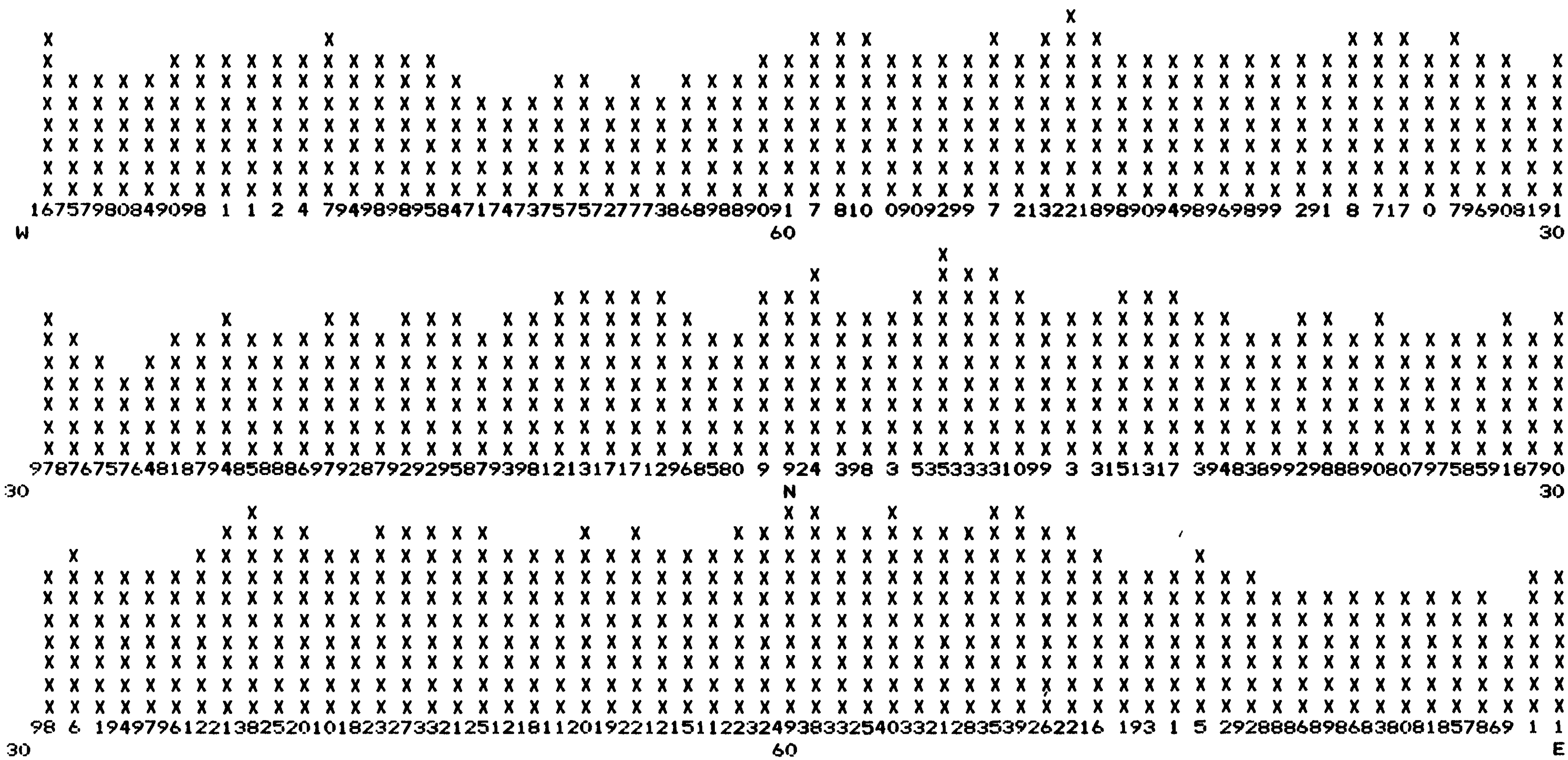

TABLE OF AZIMUTH VS FREQUENCY FOR PRECEDING STRIKE FREQUENCY PLOT

AZIM	BRNG	FREQ	AZIM	BRNG	FREQ	AZIM	BRNG	FREQ	AZIM	BRNG	FREQ
271	-89	116	316	-44	98	1	1	124	46	46	133
272	-88	75	317	-43	96	2	2	103	47	47	121
273	-87	79	318	-42	98	3	3	98	48	48	125
274	-86	80	319	-41	99	4	4	103	49	49	112
275	-85	84	320	-40	102	5	5	105	50	50	118
276	-84	90	321	-39	91	6	6	135	51	51	111
277	-83	98	322	-38	108	7	7	133	52	52	120
278	-82	101	323	-37	107	8	8	133	53	53	119
279	-81	101	324	-36	117	9	9	110	54	54	122
280	-80	102	325	-35	100	10	10	99	55	55	112
281	-79	104	326	-34	107	11	11	103	56	56	115
282	-78	107	327	-33	96	12	12	103	57	57	111
283	-77	94	328	-32	90	13	13	115	58	58	122
284	-76	98	329	-31	81	14	14	113	59	59	132
285	-75	98	330	-30	91	15	15	117	60	60	149
286	-74	95	331	-29	97	16	16	103	61	61	138
287	-73	84	332	-28	87	17	17	94	62	62	133
288	-72	71	333	-27	67	18	18	83	63	63	125
289	-71	74	334	-26	57	19	19	89	64	64	140
290	-70	73	335	-25	64	20	20	92	65	65	133
291	-69	75	336	-24	81	21	21	98	66	66	121
292	-68	75	337	-23	87	22	22	88	67	67	128
293	-67	72	338	-22	94	23	23	90	68	68	135
294	-66	77	339	-21	85	24	24	80	69	69	139
295	-65	73	340	-20	88	25	25	79	70	70	126
296	-64	86	341	-19	86	26	26	75	71	71	122
297	-63	89	342	-18	97	27	27	85	72	72	116
298	-62	88	343	-17	92	28	28	91	73	73	101
299	-61	90	344	-16	87	29	29	87	74	74	93
300	-60	91	345	-15	92	30	30	90	75	75	101
301	-59	107	346	-14	92	31	31	98	76	76	105
302	-58	108	347	-13	95	32	32	106	77	77	102
303	-57	110	348	-12	87	33	33	101	78	78	92
304	-56	100	349	-11	93	34	34	94	79	79	88
305	-55	90	350	-10	98	35	35	97	80	80	86
306	-54	92	351	-9	112	36	36	96	81	81	89
307	-53	99	352	-8	113	37	37	112	82	82	86
308	-52	107	353	-7	117	38	38	121	83	83	83
309	-51	102	354	-6	117	39	39	138	84	84	80
310	-50	113	355	-5	112	40	40	125	85	85	81
311	-49	122	356	-4	96	41	41	120	86	86	85
312	-48	118	357	-3	85	42	42	110	87	87	78
313	-47	98	358	-2	80	43	43	118	88	88	69
314	-46	90	359	-1	109	44	44	123	89	89	101
315	-45	94	360	0	109	45	45	127	90	90	101

FOUR CORNERS LINEAR FEATURES

FREQUENCY PROBABILITY DATA

NO. OF DATA = 6050 EVENT PROB. = 0.017 PROB. LIMIT = 0.970

FREQUENCY MEAN = 100.8

EMP. FREQ.	REL. FREQ.	FREQ. PROB.	SIGNIF VALUE
82	1.9	0.007	93.7
83	1.9	0.008	92.1
84	1.9	0.010	90.1
85	1.9	0.012	87.8
86	1.9	0.014	85.0
87	1.9	0.016	81.8
88	2.0	0.018	78.1
89	2.0	0.020	74.0
90	2.0	0.023	69.3
91	2.0	0.025	64.2
92	2.0	0.028	58.5
93	2.0	0.030	52.4
94	2.1	0.032	45.8
95	2.1	0.034	38.8
96	2.1	0.036	31.5
97	2.1	0.038	23.9
98	2.1	0.039	16.0
99	2.1	0.039	8.1
100	2.2	0.040	0.0
101	2.2	0.040	0.0
102	2.2	0.039	7.8
103	2.2	0.038	15.6
104	2.2	0.037	23.1
105	2.2	0.036	30.5
106	2.3	0.034	37.5
107	2.3	0.032	44.3
108	2.3	0.030	50.6
109	2.3	0.028	56.5
110	2.3	0.025	61.9
111	2.3	0.023	66.9
112	2.4	0.021	71.5
113	2.4	0.019	75.6
114	2.4	0.016	79.2
115	2.4	0.014	82.5
116	2.4	0.012	85.3
117	2.4	0.011	87.8
118	2.5	0.009	89.9
119	2.5	0.008	91.7
120	2.5	0.007	93.2

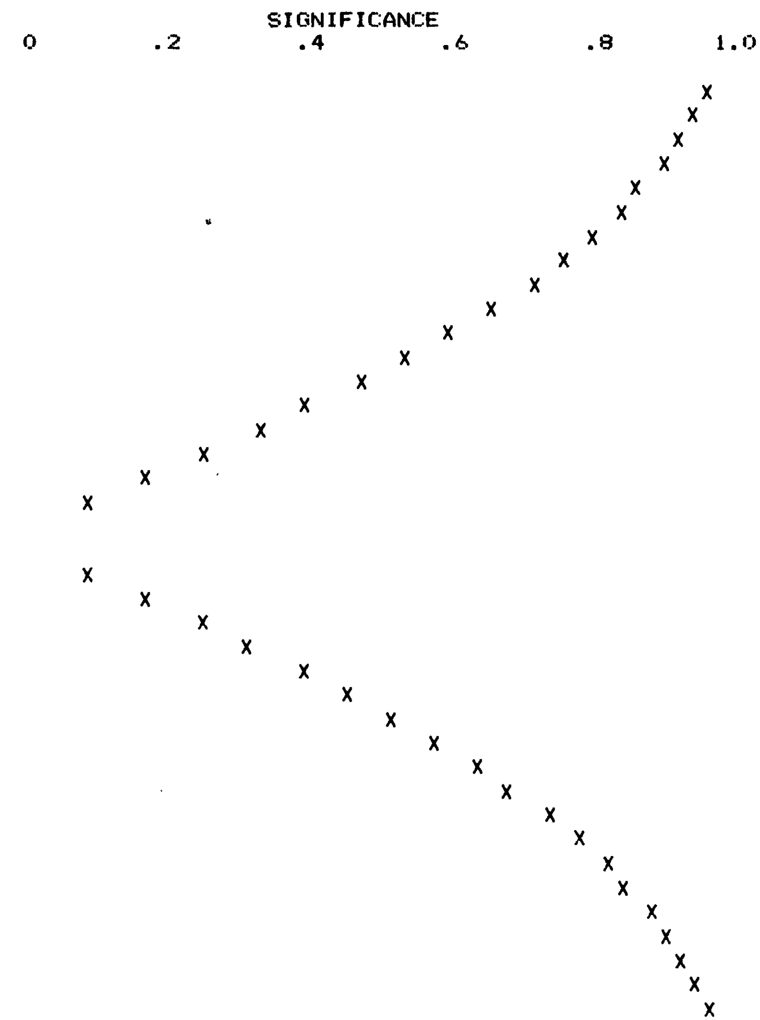

EMPIRICAL STRIKE FREQUENCY ANALYSIS.

FOUR CORNERS WEIGHTED SEGMENTS

10 LEVELS OF FREQUENCY AT   80 PER LEVEL.

PERCENT AZIMUTH FOR SMOOTHING =   1.67

NO. OF DATA = 27044

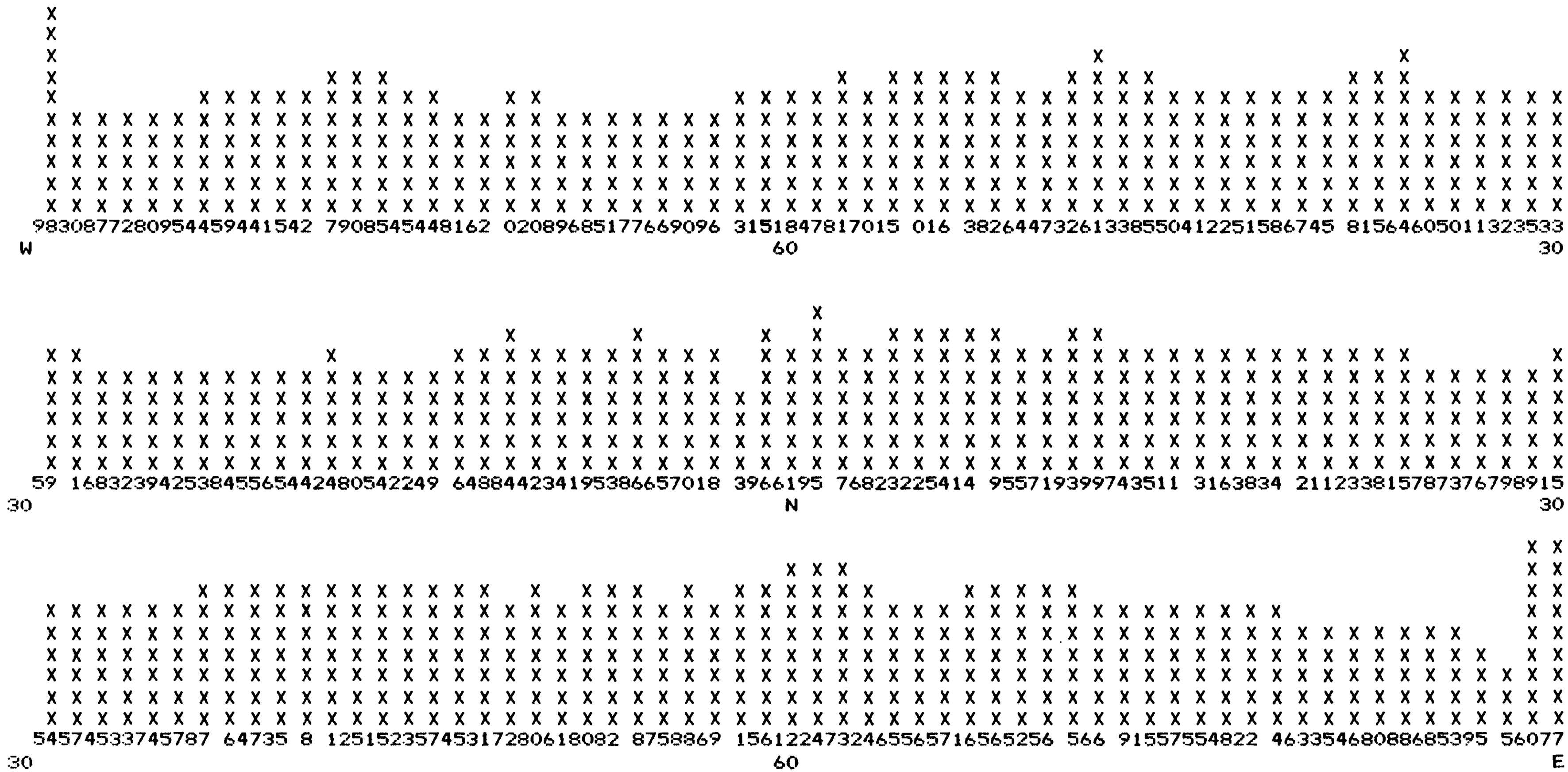

TABLE OF AZIMUTH VS FREQUENCY FOR PRECEDING STRIKE FREQUENCY PLOT

AZIM	BRNG	FREQ	AZIM	BRNG	FREQ	AZIM	BRNG	FREQ	AZIM	BRNG	FREQ
271	-89	798	316	-44	441	1	1	595	46	46	557
272	-88	330	317	-43	422	2	2	407	47	47	545
273	-87	387	318	-42	451	3	3	468	48	48	531
274	-86	372	319	-41	458	4	4	523	49	49	472
275	-85	380	320	-40	467	5	5	522	50	50	480
276	-84	395	321	-39	445	6	6	554	51	51	461
277	-83	444	322	-38	508	7	7	514	52	52	480
278	-82	459	323	-37	515	8	8	509	53	53	482
279	-81	444	324	-36	564	9	9	455	54	54	508
280	-80	415	325	-35	460	10	10	471	55	55	475
281	-79	442	326	-34	450	11	11	493	56	56	488
282	-78	507	327	-33	411	12	12	499	57	57	469
283	-77	490	328	-32	432	13	13	474	58	58	501
284	-76	485	329	-31	435	14	14	435	59	59	556
285	-75	445	330	-30	433	15	15	411	60	60	612
286	-74	444	331	-29	459	16	16	403	61	61	624
287	-73	381	332	-28	401	17	17	416	62	62	573
288	-72	362	333	-27	368	18	18	438	63	63	524
289	-71	400	334	-26	332	19	19	434	64	64	465
290	-70	420	335	-25	339	20	20	402	65	65	456
291	-69	389	336	-24	342	21	21	411	66	66	457
292	-68	368	337	-23	353	22	22	423	67	67	516
293	-67	351	338	-22	384	23	23	438	68	68	556
294	-66	377	339	-21	355	24	24	415	69	69	552
295	-65	366	340	-20	365	25	25	378	70	70	556
296	-64	390	341	-19	344	26	26	373	71	71	505
297	-63	396	342	-18	424	27	27	376	72	72	466
298	-62	403	343	-17	380	28	28	379	73	73	409
299	-61	415	344	-16	354	29	29	389	74	74	415
300	-60	418	345	-15	322	30	30	415	75	75	457
301	-59	447	346	-14	349	31	31	454	76	76	455
302	-58	481	347	-13	406	32	32	457	77	77	448
303	-57	470	348	-12	448	33	33	445	78	78	422
304	-56	515	349	-11	484	34	34	433	79	79	404
305	-55	500	350	-10	442	35	35	474	80	80	363
306	-54	516	351	-9	434	36	36	457	81	81	335
307	-53	503	352	-8	419	37	37	487	82	82	346
308	-52	482	353	-7	453	38	38	506	83	83	380
309	-51	464	354	-6	486	39	39	547	84	84	388
310	-50	447	355	-5	465	40	40	535	85	85	368
311	-49	532	356	-4	470	41	41	508	86	86	353
312	-48	561	357	-3	418	42	42	501	87	87	295
313	-47	533	358	-2	303	43	43	525	88	88	205
314	-46	485	359	-1	496	44	44	515	89	89	660
315	-45	450	360	0	461	45	45	523	90	90	677

FOUR CORNERS WEIGHTED SEGMENTS

FREQUENCY PROBABILITY DATA

NO. OF DATA = 27044 EVENT PROB. = 0.017 PROB. LIMIT = 0.970

FREQUENCY MEAN = 450.7

EMP. FREQ.	REL. FREQ.	FREQ. PROB.	SIGNIF VALUE
411	2.0	0.003	93.8
412	2.0	0.004	93.1
413	2.0	0.004	92.3
414	2.0	0.004	91.5
415	2.0	0.005	90.6
416	2.0	0.005	89.6
417	2.0	0.005	88.5
418	2.0	0.006	87.3
419	2.0	0.006	86.1
420	2.1	0.007	84.8
421	2.1	0.007	83.3
422	2.1	0.008	81.8
423	2.1	0.008	80.2
424	2.1	0.009	78.5
425	2.1	0.009	76.6
426	2.1	0.010	74.7
427	2.1	0.010	72.6
428	2.1	0.011	70.5
429	2.1	0.011	68.2
430	2.1	0.012	65.8
431	2.1	0.012	63.3
432	2.1	0.013	60.8
433	2.1	0.013	58.1
434	2.1	0.014	55.3
435	2.1	0.014	52.4
436	2.1	0.015	49.3
437	2.1	0.015	46.3
438	2.1	0.016	43.1
439	2.1	0.016	39.8
440	2.1	0.017	36.4
441	2.1	0.017	33.0
442	2.1	0.017	29.5
443	2.1	0.018	26.0
444	2.1	0.018	22.4
445	2.1	0.018	18.7
446	2.1	0.018	15.0
447	2.2	0.019	11.3
448	2.2	0.019	7.5
449	2.2	0.019	3.8
450	2.2	0.019	0.0
451	2.2	0.019	0.0
452	2.2	0.019	3.7
453	2.2	0.019	7.5
454	2.2	0.019	11.2
455	2.2	0.018	14.9
456	2.2	0.018	18.5
457	2.2	0.018	22.2
458	2.2	0.018	25.7
459	2.2	0.017	29.2
[illegible]	[illegible]	0.017	32.7

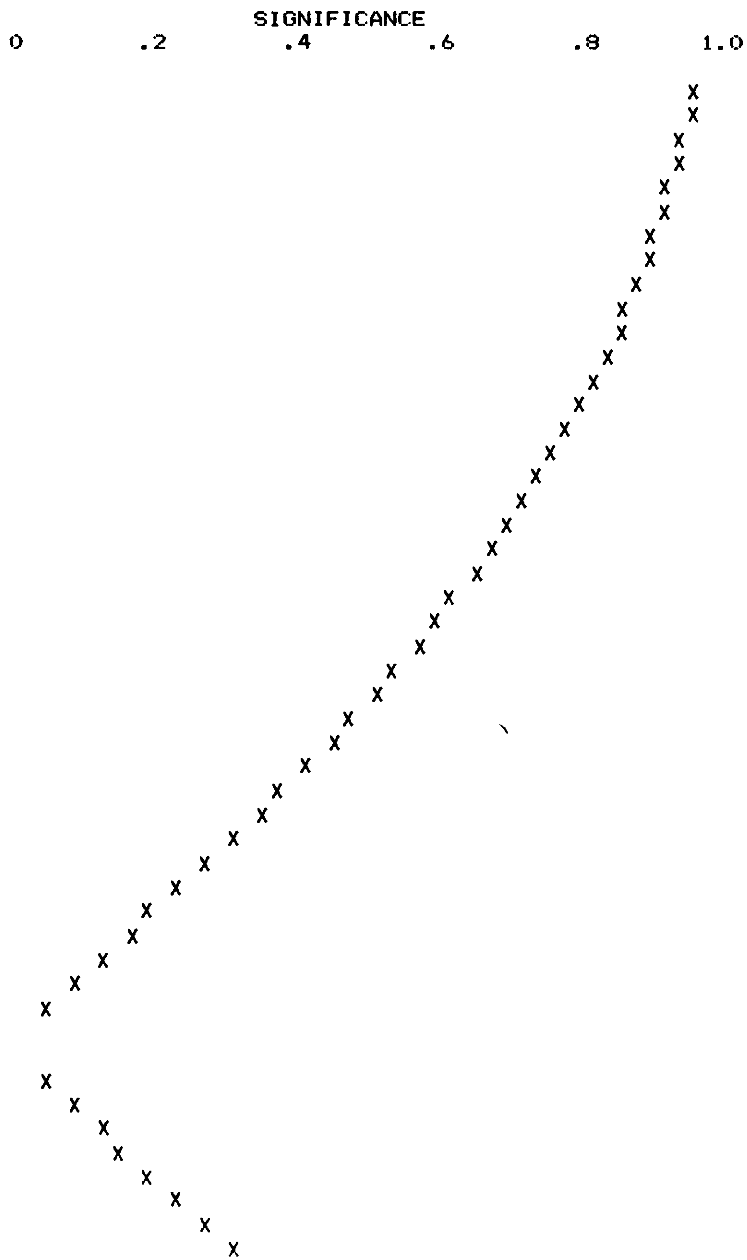

462	2.2	0.016	39.3
463	2.2	0.016	42.6
464	2.2	0.015	45.7
465	2.2	0.015	48.7
466	2.2	0.014	51.7
467	2.2	0.014	54.5
468	2.2	0.013	57.3
469	2.2	0.013	60.0
470	2.2	0.012	62.5
471	2.2	0.012	65.0
472	2.2	0.011	67.3
473	2.2	0.011	69.5
474	2.3	0.010	71.7
475	2.3	0.010	73.7
476	2.3	0.009	75.6
477	2.3	0.009	77.4
478	2.3	0.008	79.1
479	2.3	0.008	80.8
480	2.3	0.007	82.3
481	2.3	0.007	83.7
482	2.3	0.006	85.1
483	2.3	0.006	86.3
484	2.3	0.005	87.5
485	2.3	0.005	88.6
486	2.3	0.005	89.6
487	2.3	0.004	90.5
488	2.3	0.004	91.4
489	2.3	0.004	92.2
490	2.3	0.003	93.0
491	2.3	0.003	93.6

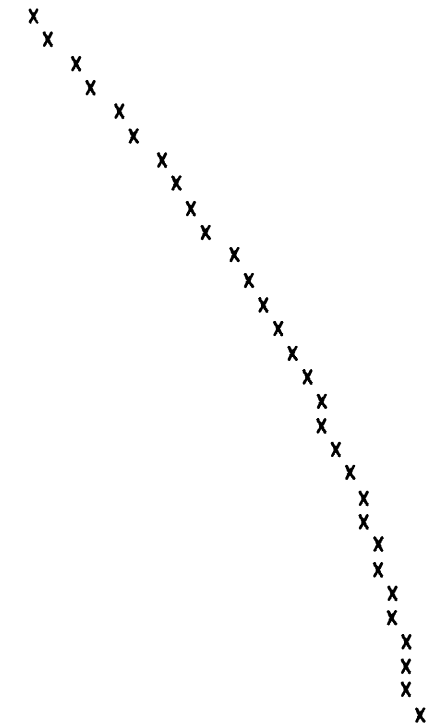

EMPIRICAL STRIKE FREQUENCY ANALYSIS.

FOUR CORNERS SEGMENTS

10 LEVELS OF FREQUENCY AT 34 PER LEVEL.

PERCENT AZIMUTH FOR SMOOTHING = 1.67

NO. OF DATA = 11255

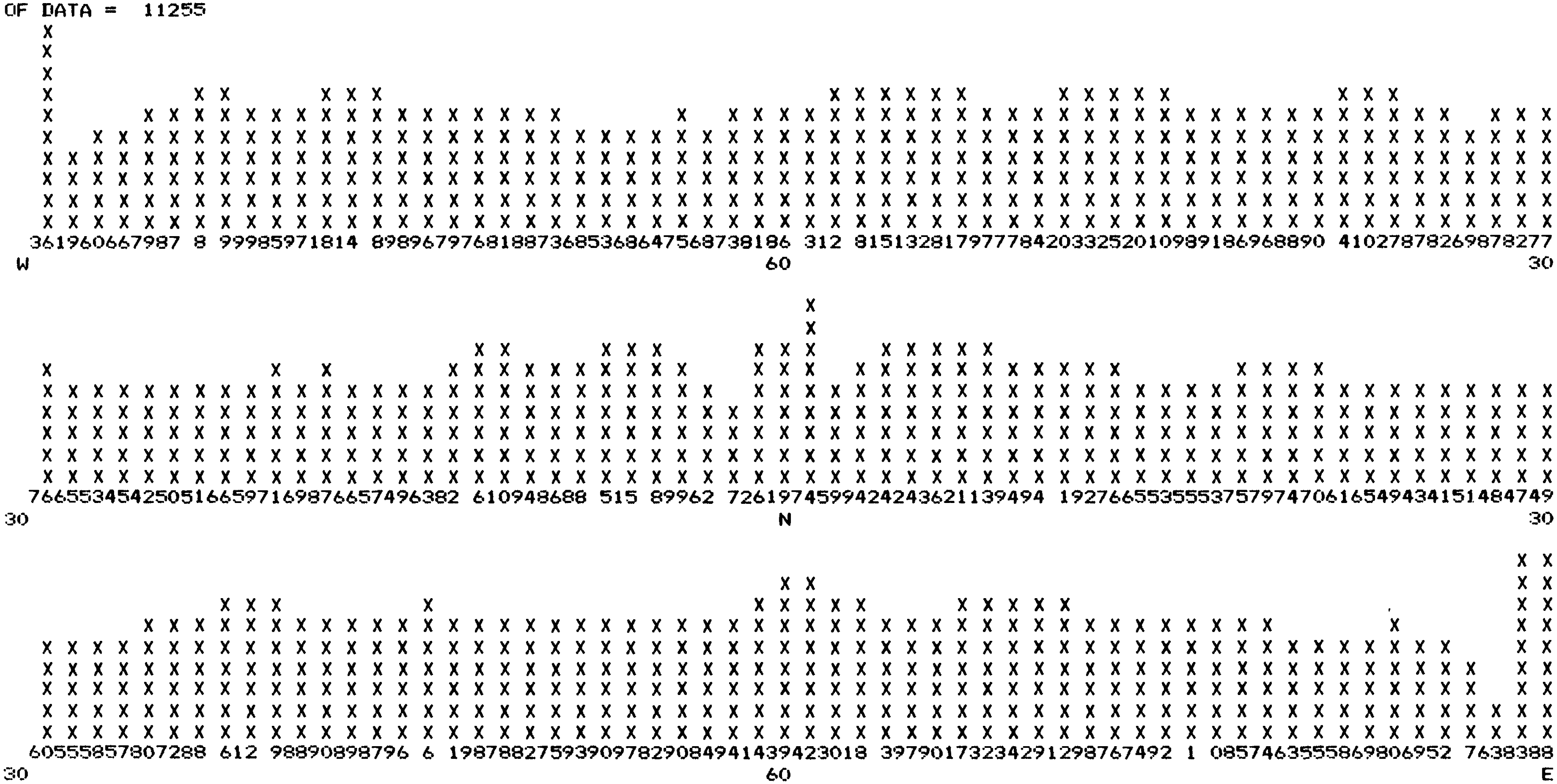

TABLE OF AZIMUTH VS FREQUENCY FOR PRECEDING STRIKE FREQUENCY PLOT

AZIM	BRNG	FREQ	AZIM	BRNG	FREQ	AZIM	BRNG	FREQ	AZIM	BRNG	FREQ
271	-89	336	316	-44	198	1	1	274	46	46	206
272	-88	119	317	-43	191	2	2	159	47	47	201
273	-87	160	318	-42	186	3	3	194	48	48	198
274	-86	166	319	-41	196	4	4	224	49	49	178
275	-85	179	320	-40	188	5	5	224	50	50	182
276	-84	187	321	-39	190	6	6	236	51	51	175
277	-83	208	322	-38	204	7	7	221	52	52	193
278	-82	209	323	-37	210	8	8	213	53	53	190
279	-81	199	324	-36	227	9	9	194	54	54	197
280	-80	185	325	-35	187	10	10	194	55	55	182
281	-79	197	326	-34	182	11	11	201	56	56	190
282	-78	218	327	-33	169	12	12	192	57	57	184
283	-77	214	328	-32	187	13	13	176	58	58	194
284	-76	208	329	-31	182	14	14	165	59	59	214
285	-75	198	330	-30	177	15	15	153	60	60	239
286	-74	196	331	-29	176	16	16	155	61	61	242
287	-73	179	332	-28	165	17	17	153	62	62	230
288	-72	176	333	-27	153	18	18	175	63	63	218
289	-71	181	334	-26	145	19	19	179	64	64	203
290	-70	188	335	-25	142	20	20	174	65	65	197
291	-69	173	336	-24	150	21	21	170	66	66	190
292	-68	168	337	-23	151	22	22	161	67	67	217
293	-67	153	338	-22	166	23	23	165	68	68	232
294	-66	168	339	-21	159	24	24	149	69	69	234
295	-65	164	340	-20	171	25	25	143	70	70	229
296	-64	175	341	-19	169	26	26	141	71	71	212
297	-63	168	342	-18	187	27	27	151	72	72	198
298	-62	173	343	-17	166	28	28	148	73	73	176
299	-61	181	344	-16	157	29	29	147	74	74	174
300	-60	186	345	-15	149	30	30	149	75	75	192
301	-59	203	346	-14	163	31	31	160	76	76	201
302	-58	212	347	-13	182	32	32	155	77	77	200
303	-57	208	348	-12	206	33	33	158	78	78	185
304	-56	215	349	-11	210	34	34	157	79	79	174
305	-55	213	350	-10	194	35	35	180	80	80	163
306	-54	228	351	-9	186	36	36	172	81	81	155
307	-53	217	352	-8	188	37	37	188	82	82	158
308	-52	197	353	-7	205	38	38	206	83	83	169
309	-51	177	354	-6	215	39	39	212	84	84	180
310	-50	184	355	-5	208	40	40	209	85	85	169
311	-49	220	356	-4	199	41	41	188	86	86	152
312	-48	233	357	-3	162	42	42	190	87	87	107
313	-47	225	358	-2	107	43	43	189	88	88	63
314	-46	220	359	-1	226	44	44	187	89	89	283
315	-45	210	360	0	219	45	45	196	90	90	288

FOUR CORNERS SEGMENTS

FREQUENCY PROBABILITY DATA

NO. OF DATA = 11255 EVENT PROB. = 0.017 PROB. LIMIT = 0.970

FREQUENCY MEAN = 187.6

EMP. FREQ.	REL. FREQ.	FREQ. PROB.	SIGNIF VALUE
162	1.9	0.005	93.8
163	1.9	0.006	92.6
164	2.0	0.007	91.3
165	2.0	0.008	89.8
166	2.0	0.009	88.1
167	2.0	0.010	86.2
168	2.0	0.011	84.1
169	2.0	0.012	81.7
170	2.0	0.013	79.1
171	2.0	0.014	76.3
172	2.0	0.016	73.2
173	2.0	0.017	69.8
174	2.0	0.018	66.2
175	2.1	0.020	62.3
176	2.1	0.021	58.1
177	2.1	0.022	53.7
178	2.1	0.023	49.1
179	2.1	0.024	44.2
180	2.1	0.025	39.2
181	2.1	0.026	33.9
182	2.1	0.027	28.5
183	2.1	0.028	23.0
184	2.1	0.028	17.3
185	2.1	0.029	11.6
186	2.2	0.029	5.8
187	2.2	0.029	0.0
188	2.2	0.029	0.0
189	2.2	0.029	5.8
190	2.2	0.028	11.6
191	2.2	0.028	17.4
192	2.2	0.027	23.0
193	2.2	0.027	28.5
194	2.2	0.026	33.8
195	2.2	0.025	39.0
196	2.2	0.024	43.9
197	2.3	0.023	48.7
198	2.3	0.021	53.2
199	2.3	0.020	57.5
200	2.3	0.019	61.6
201	2.3	0.018	65.3
202	2.3	0.016	68.9
203	2.3	0.015	72.2
204	2.3	0.014	75.2
205	2.3	0.013	78.0
206	2.3	0.012	80.5
207	2.3	0.010	82.9
208	2.3	0.009	85.0
209	2.4	0.008	86.9
210	2.4	0.008	88.6
211	2.4	0.007	90.1
213	2.4	0.005	92.7
214	2.4	0.005	93.7

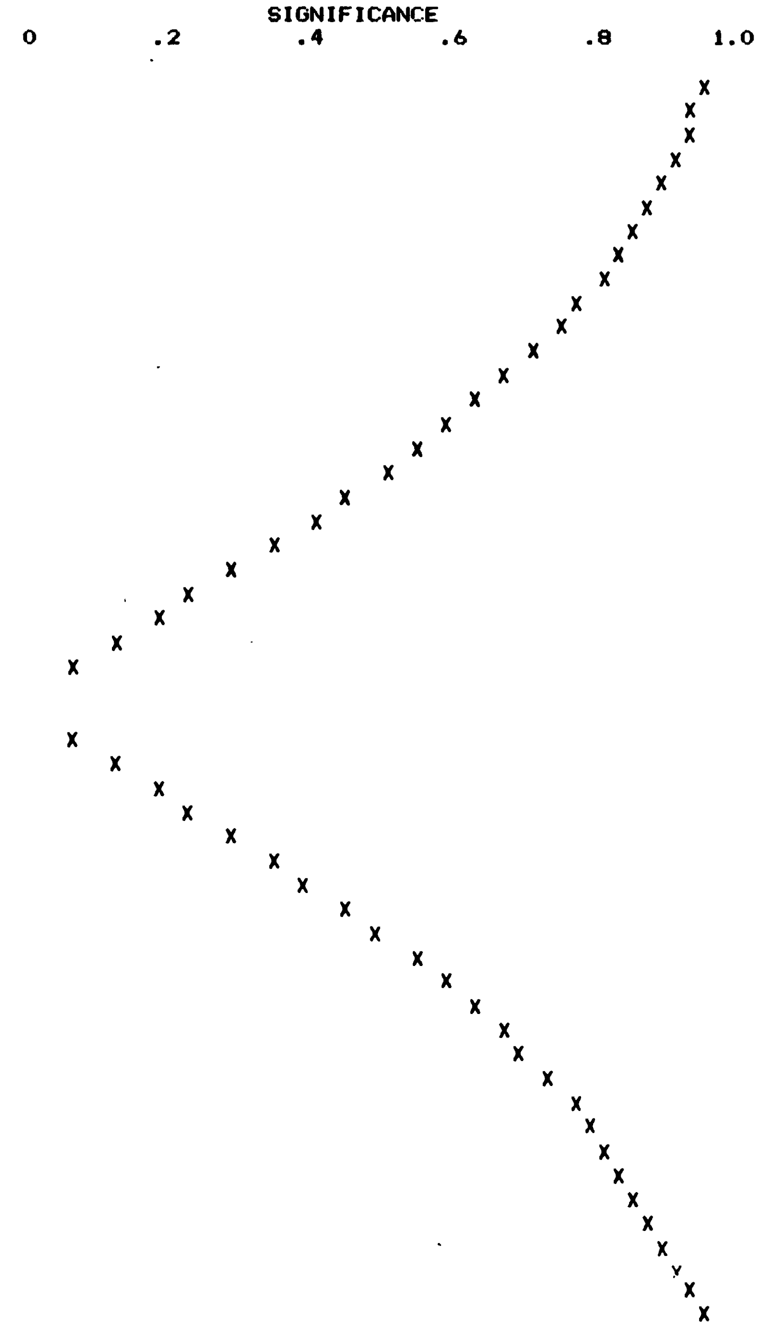

Computer-generated Maps of Linear Features in Important Azimuthal Trend Intervals

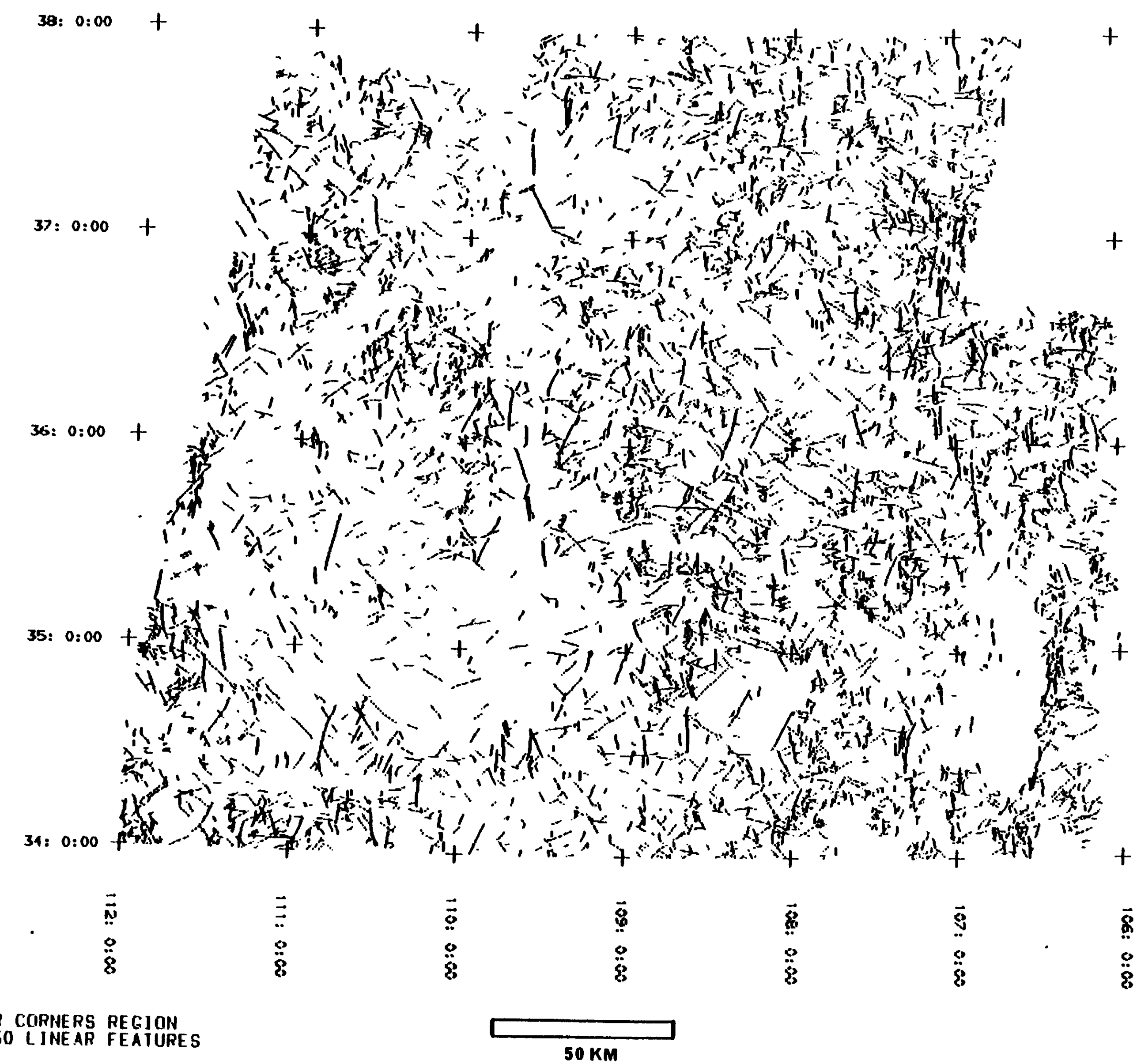

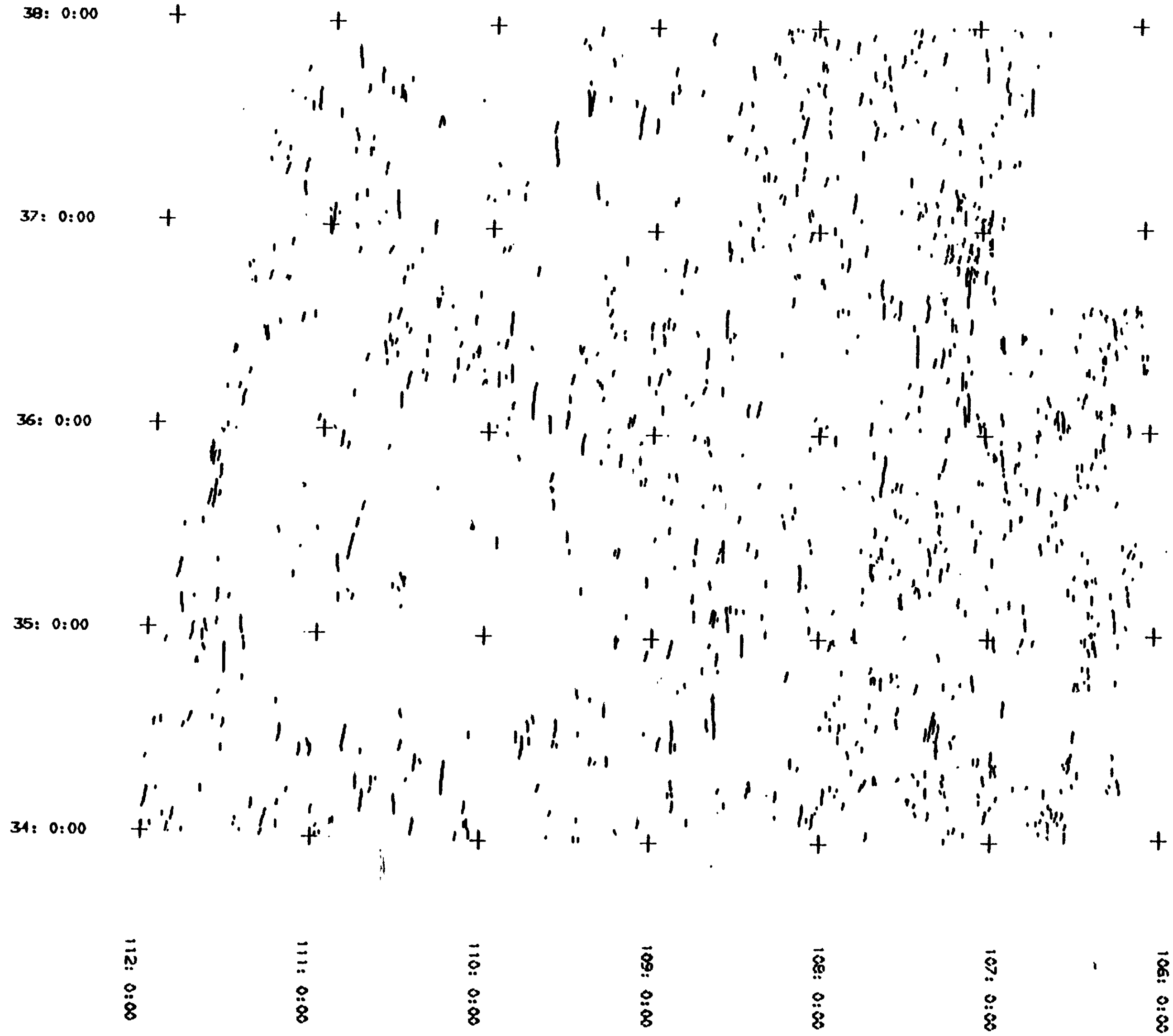

FOUR CORNERS REGION
N10W-16E; NORTH TREND INTERVAL

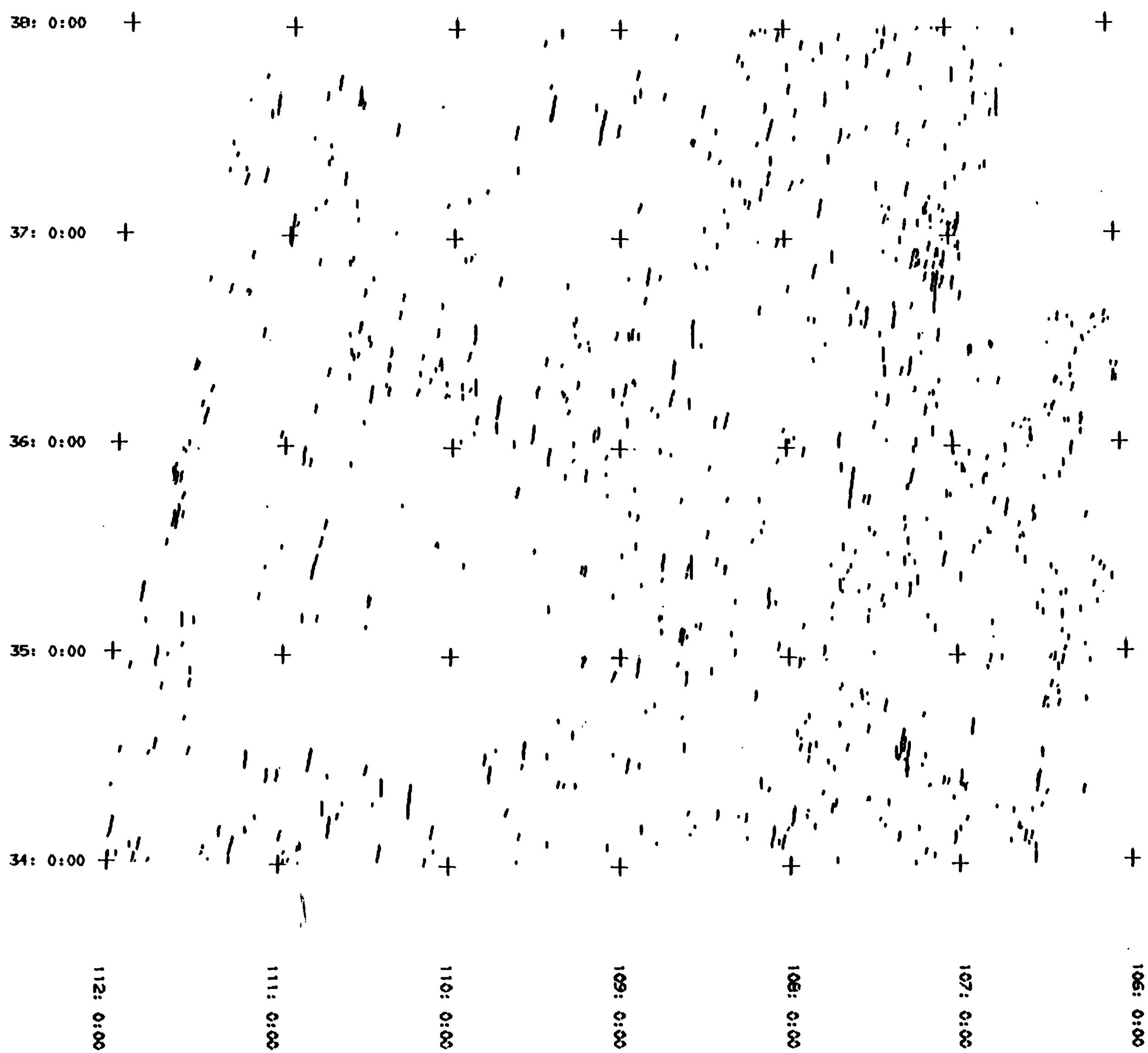

NO-16E LINEAR FEATURES
FOUR CORNERS REGION

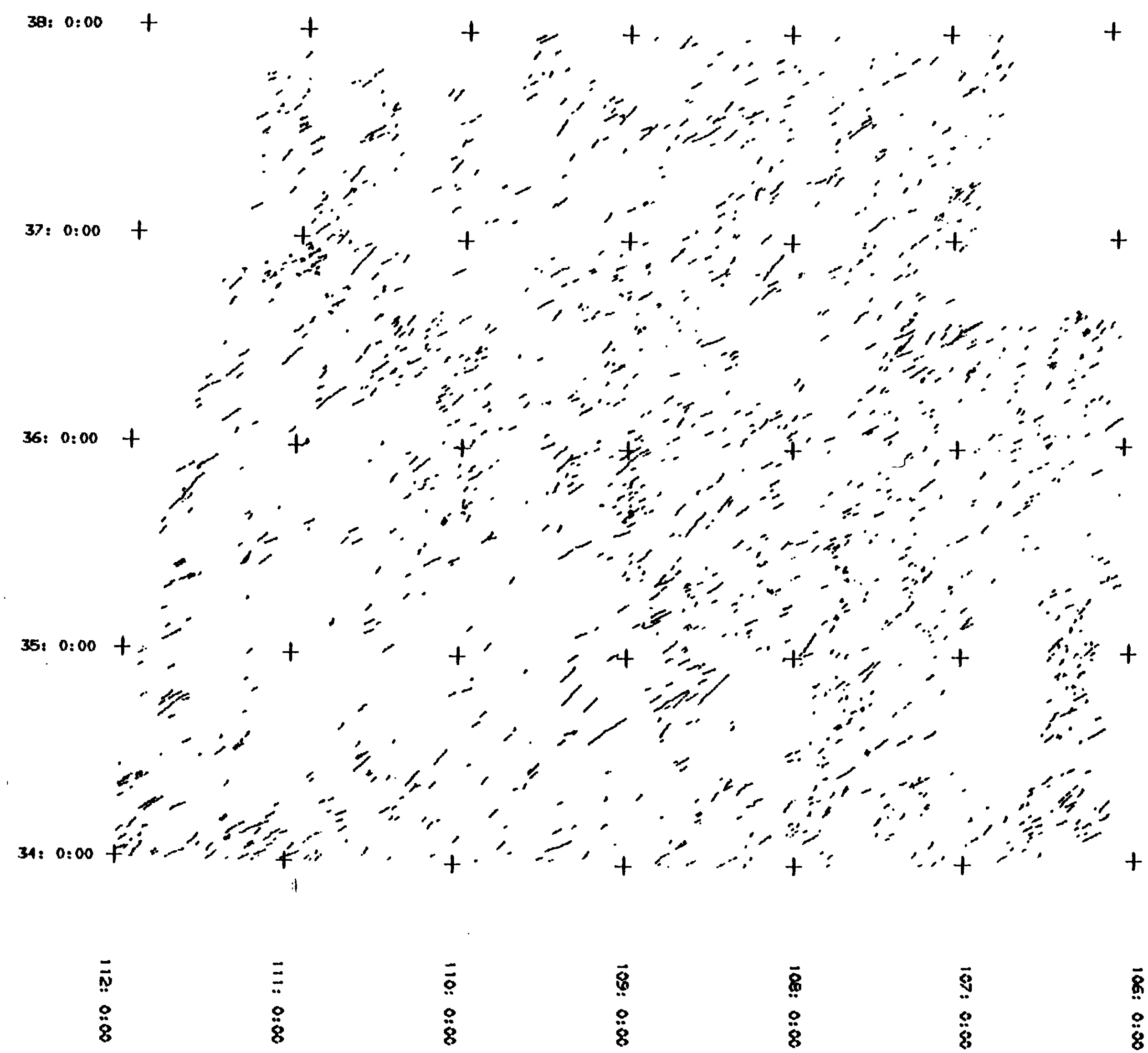

N35-72E LINEAR FEATURES
FOUR CORNERS REGION

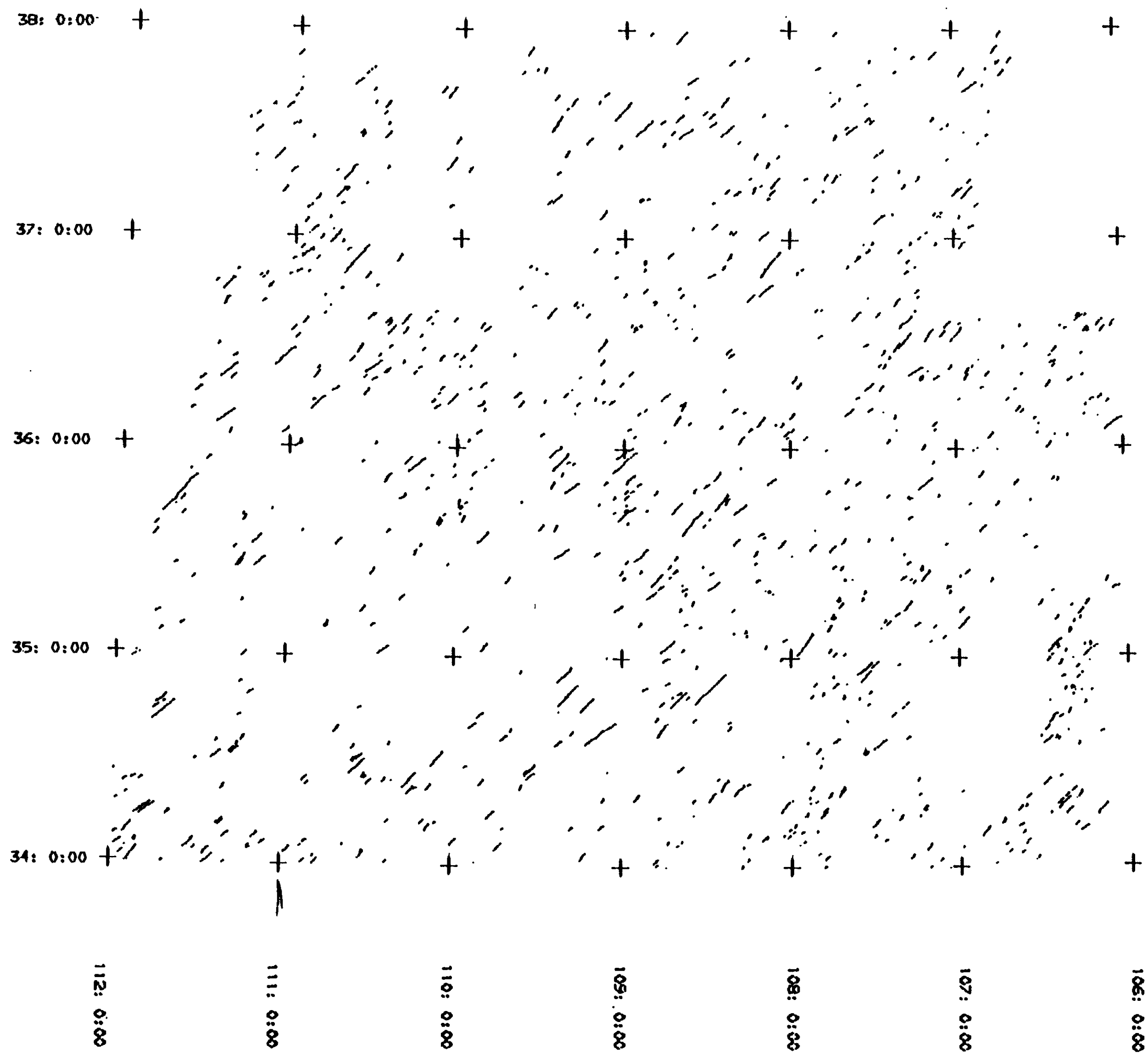

N35-57E LINEAR FEATURES
FOUR CORNERS REGION

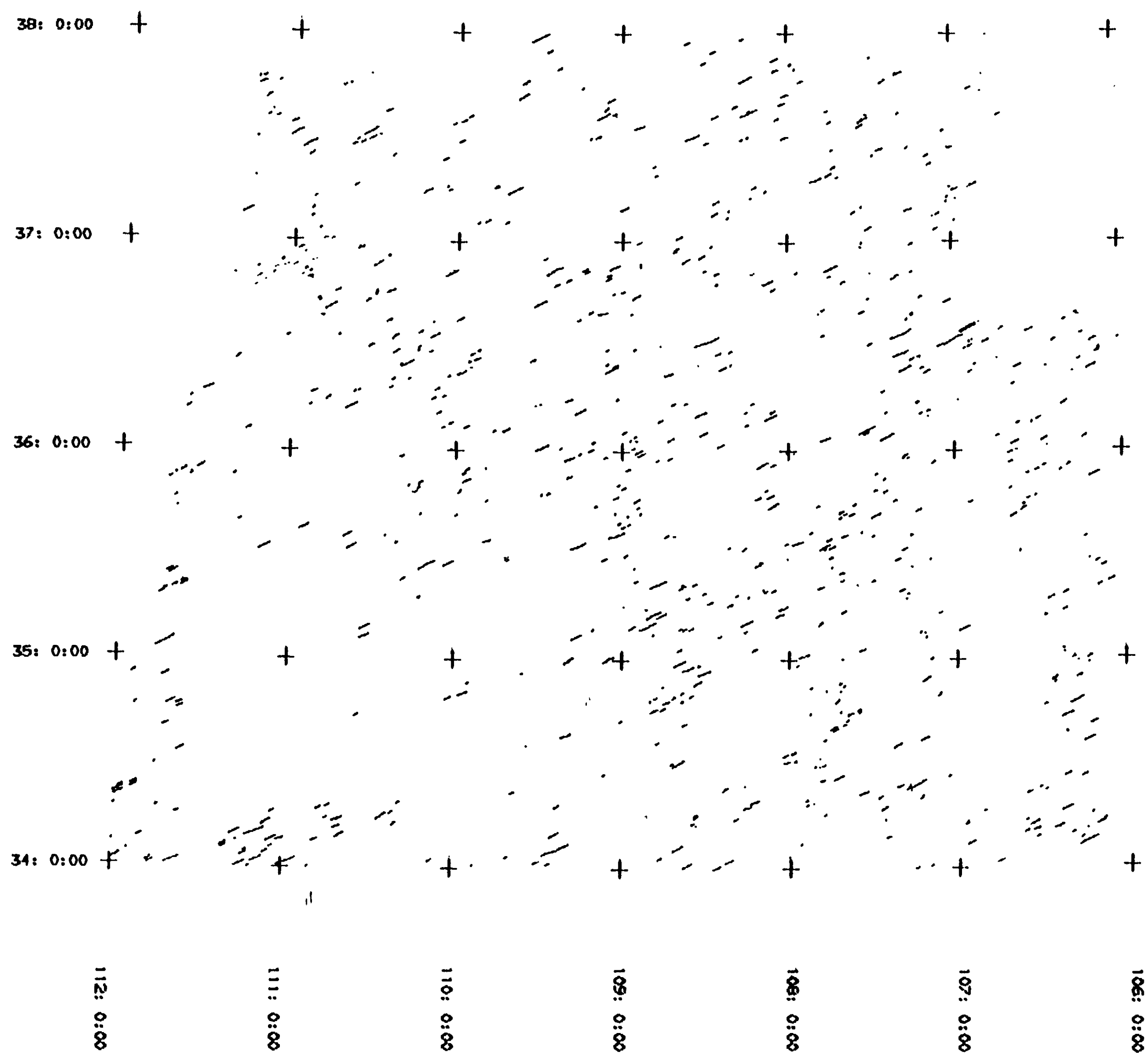

W58-72E LINEAR FEATURES
FOUR CORNERS REGION

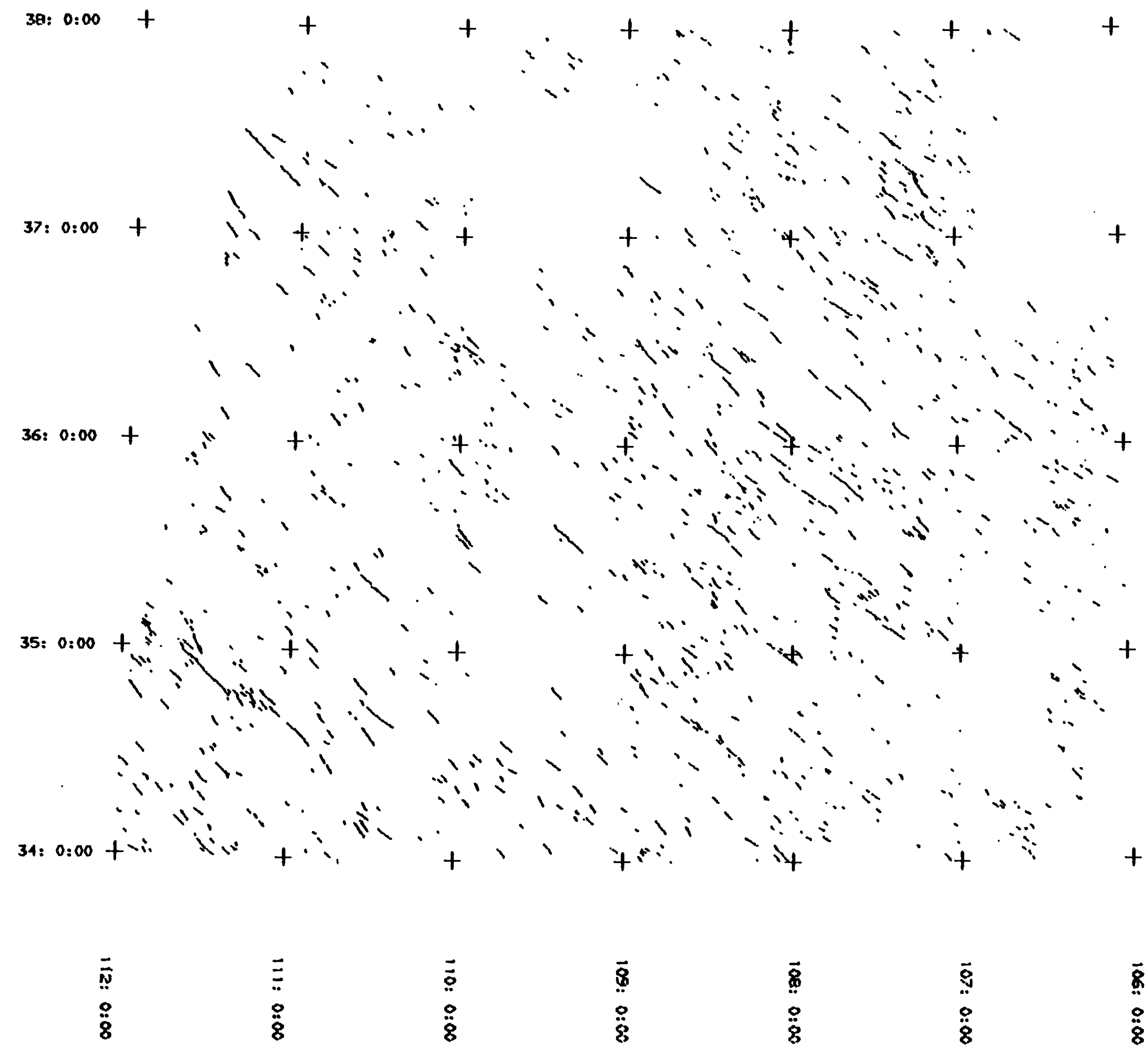

N33-59W LINEAR FEATURES
FOUR CORNERS REGION

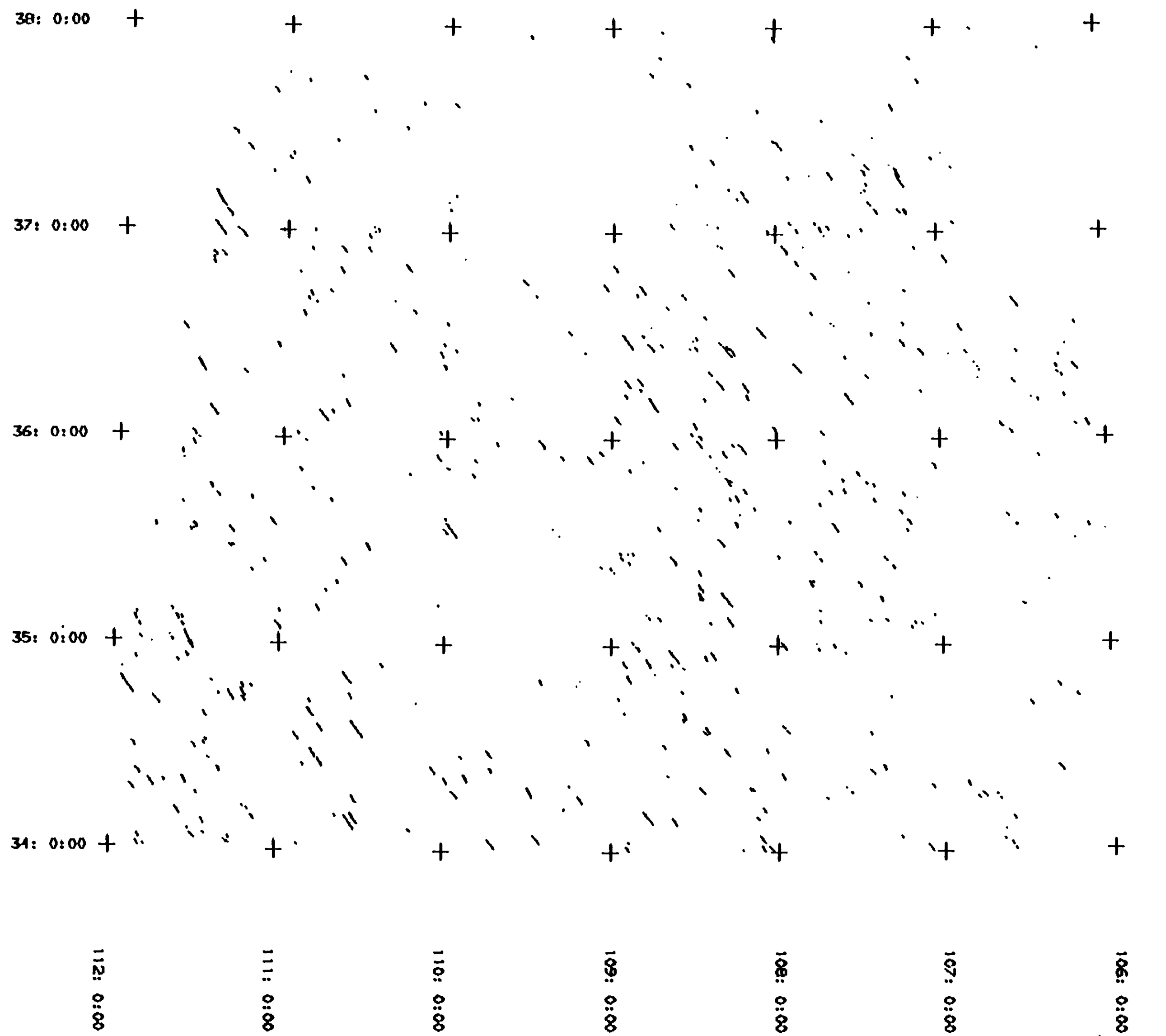

N33-43W LINEAR FEATURES
FOUR CORNERS REGION

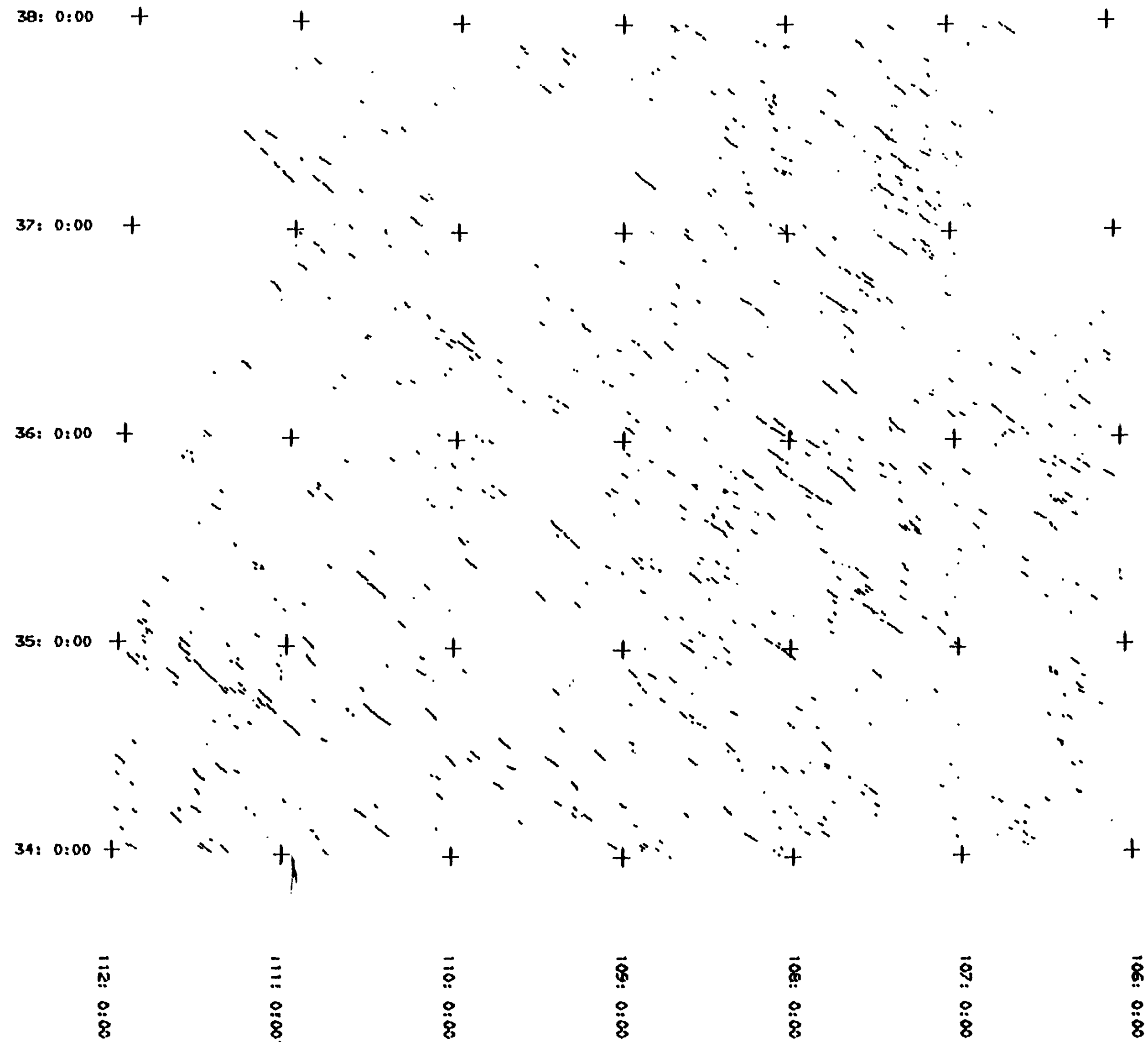

N43-59W LINEAR FEATURES
FOUR CORNERS REGION

Computer-generated Contour Maps of Linear Feature Concentrations in Important Azimuthal Trend Intervals

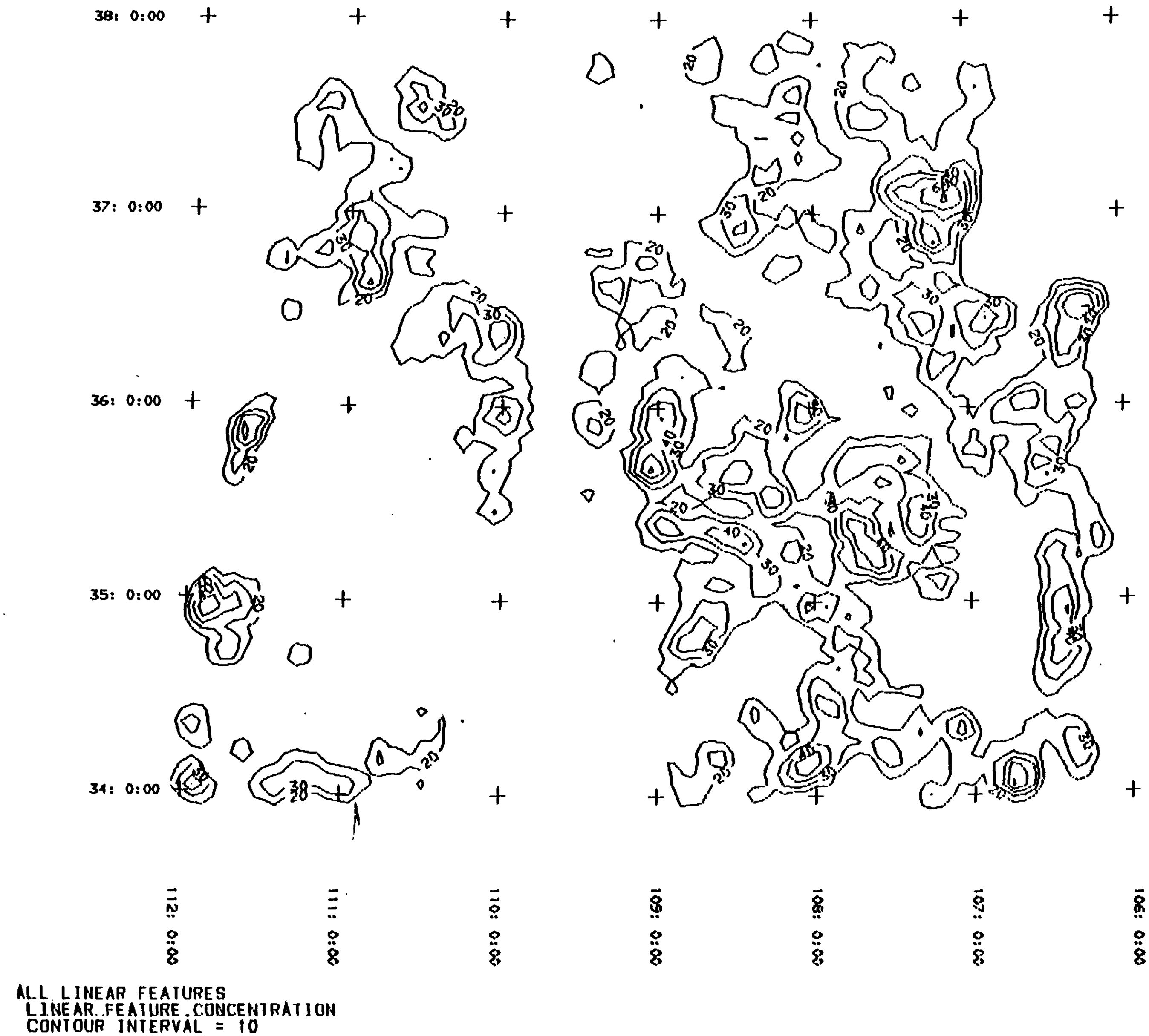

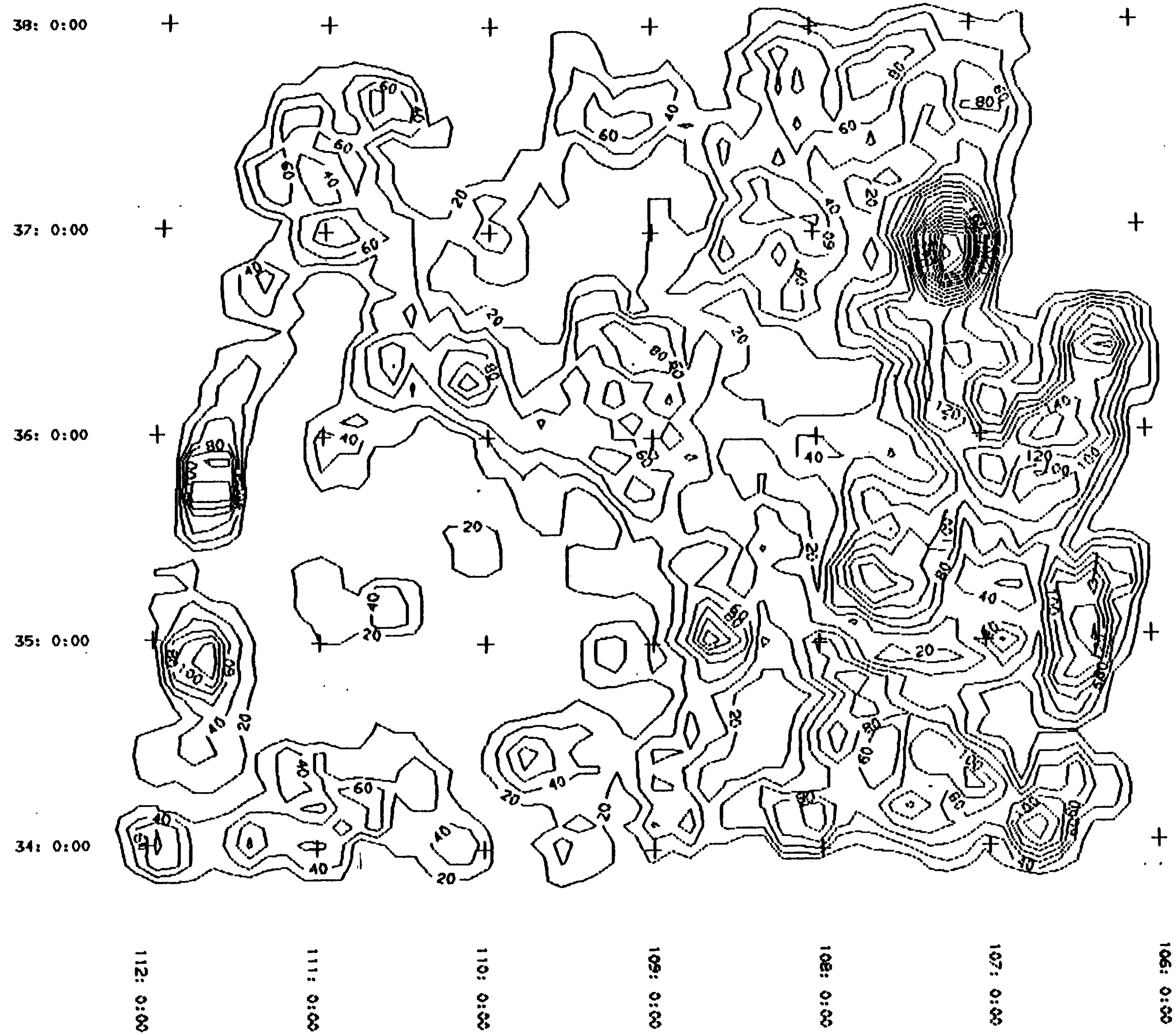

FOUR CORNERS REGION
LINEAR FEATURE CONCENTRATION
N10W-16E; I=1; D=10; CI=20

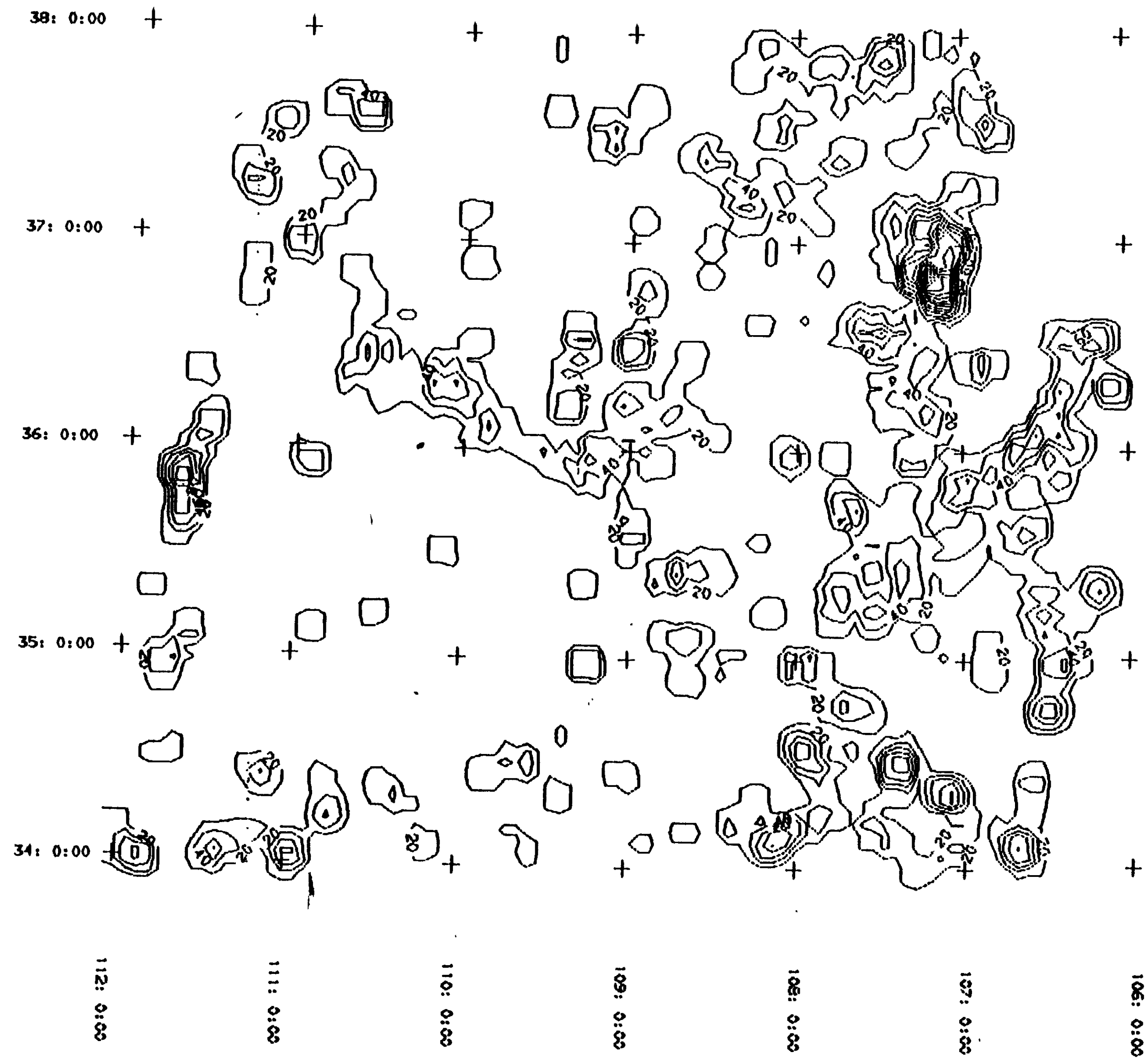

NO-16E I=1; D=6
LINEAR FEATURE CONCENTRATION
CONTOUR INTERVAL= 20

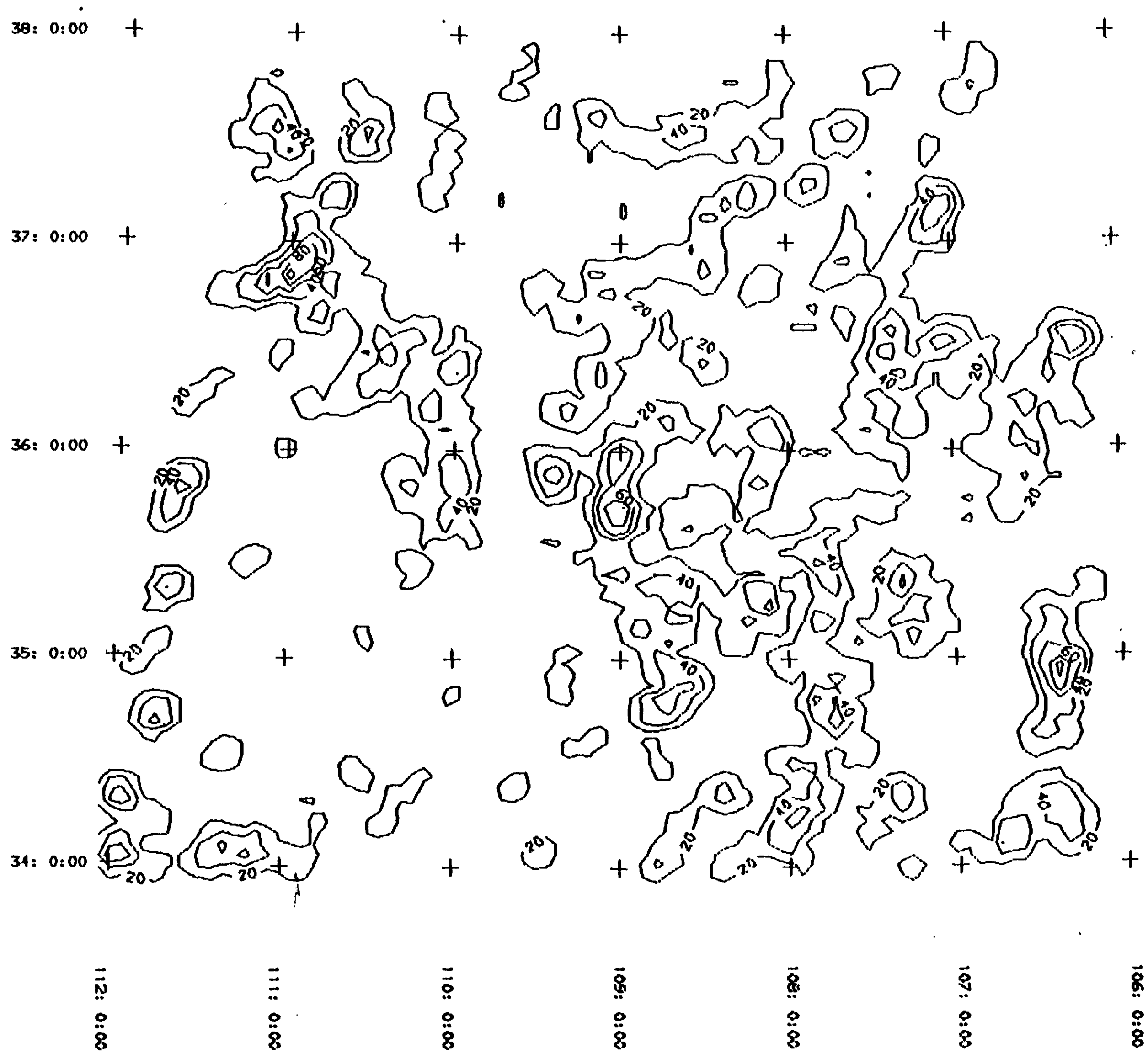

N35-72E I=1; D=6
LINEAR FEATURE CONCENTRATION
CONTOUR INTERVAL=20

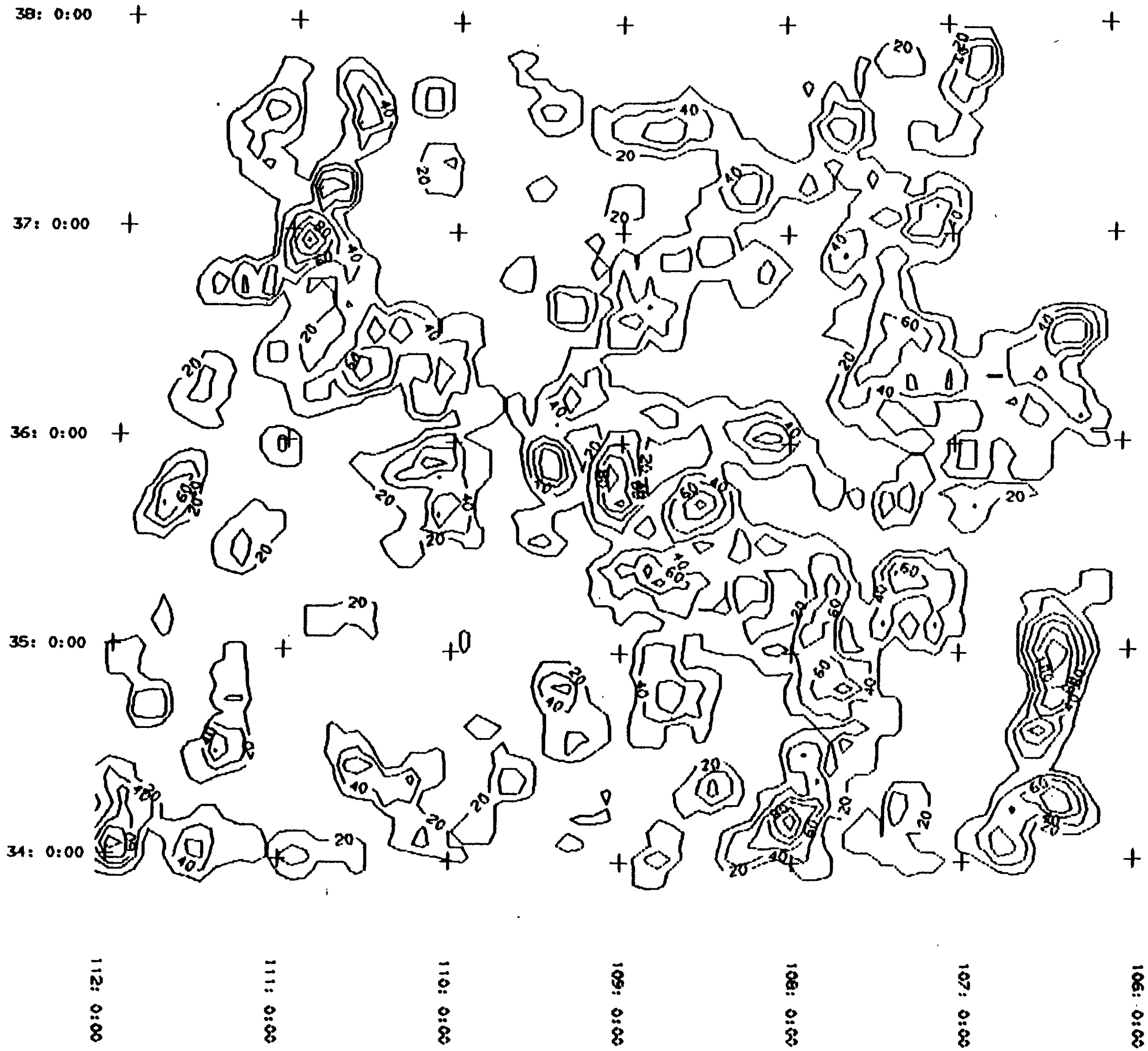

N35-57E I=1; D=7
LINEAR FEATURE CONCENTRATION
CONTOUR INTERVAL=20

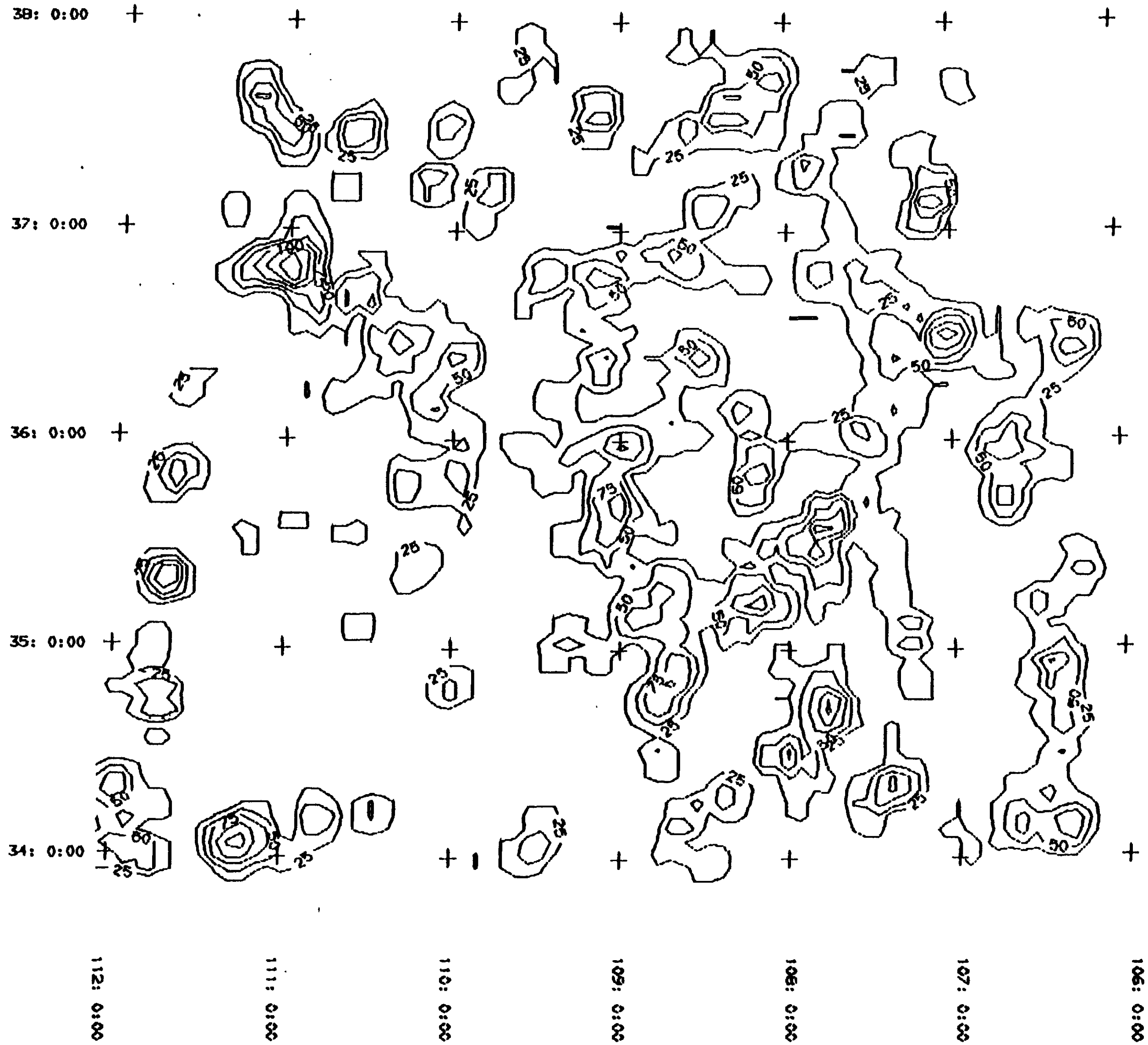

N58-72E I=1; D=7
LINEAR FEATURE CONCENTRATION
CONTOUR INTERVAL=25

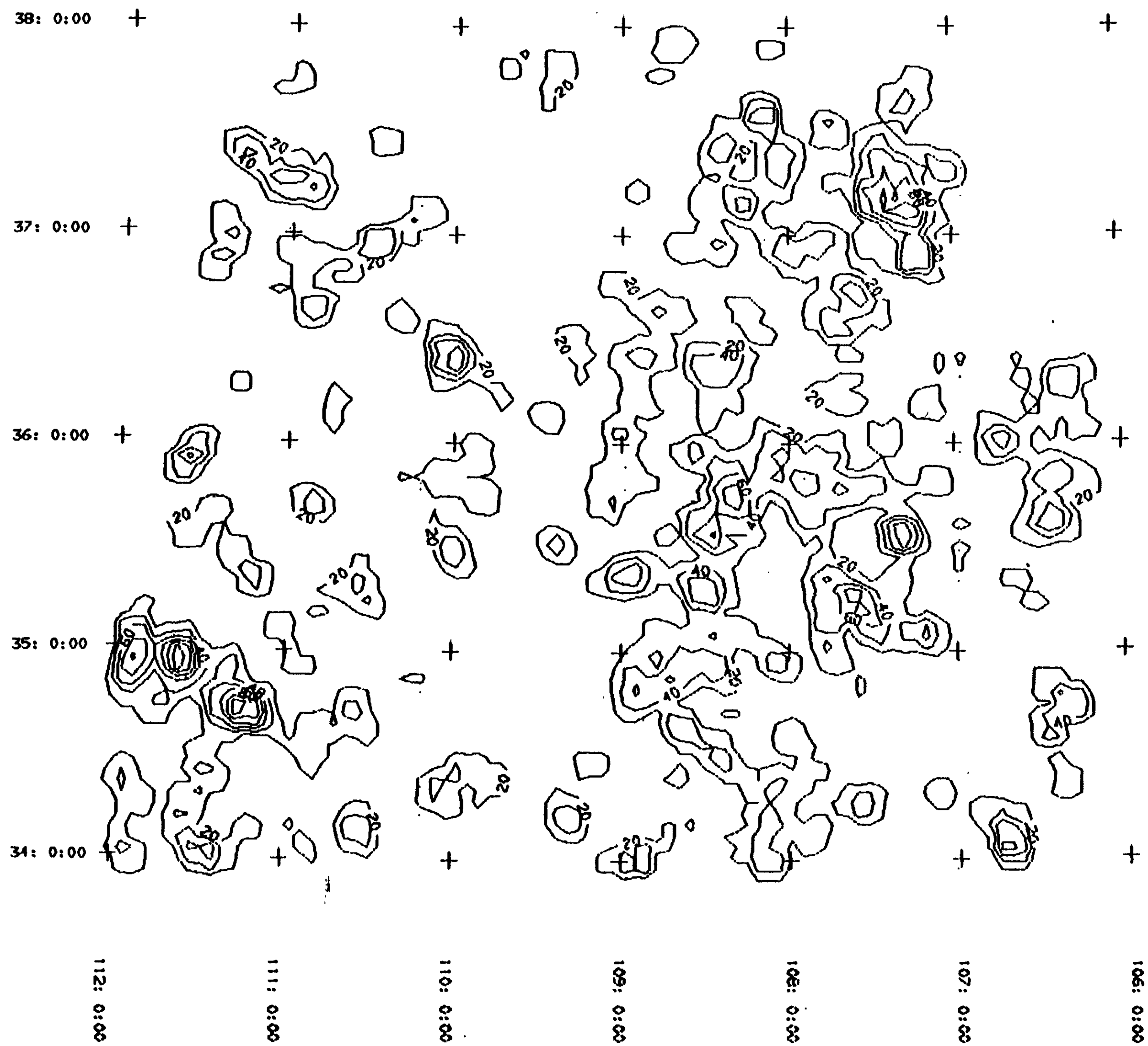

N33-59W I=1; D=6
LINEAR FEATURE CONCENTRATION
CONTOUR INTERVAL = 20

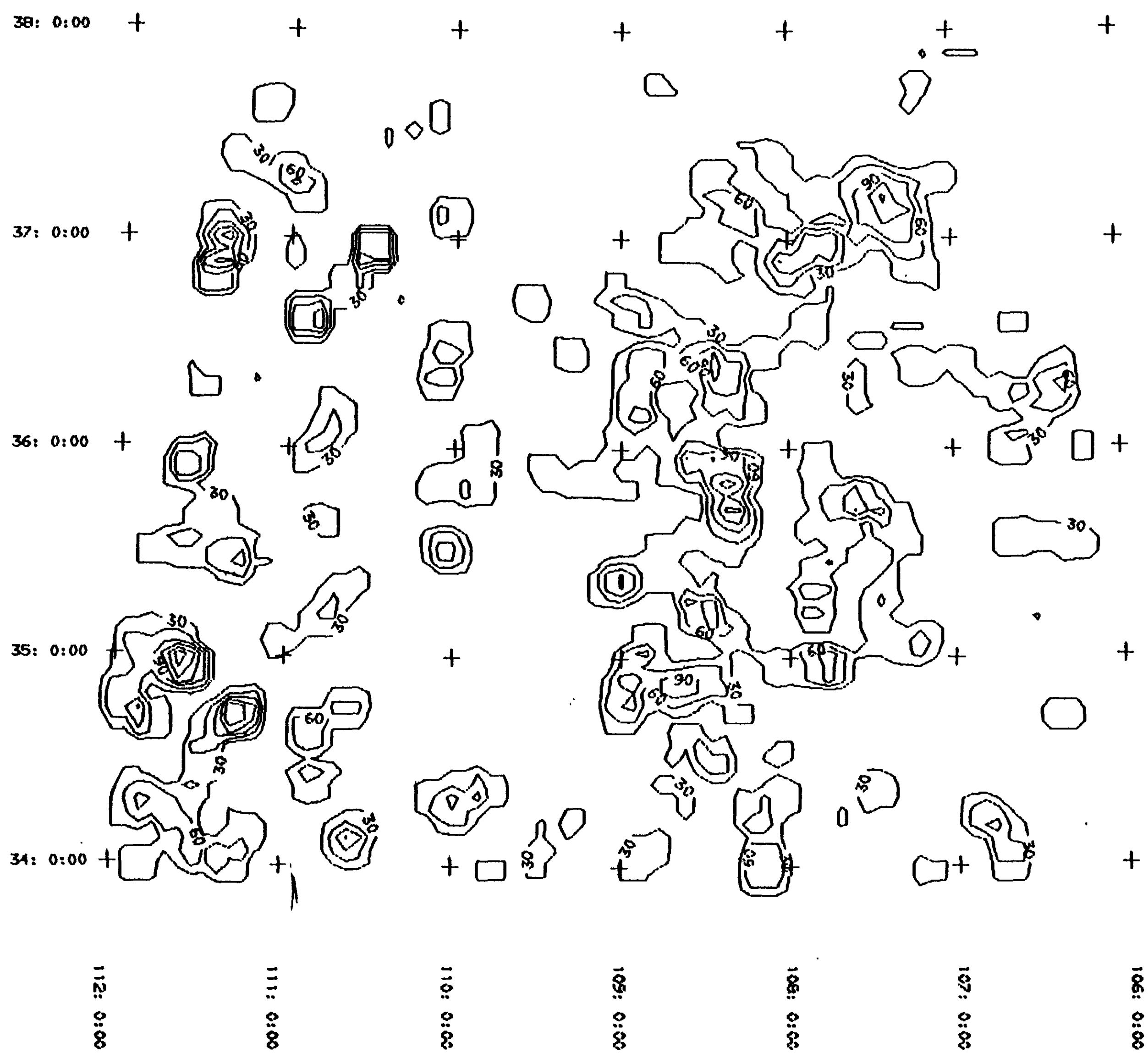

N33-43W I=1; D=7
LINEAR FEATURE CONCENTRATION
CONTOUR INTERVAL = 30

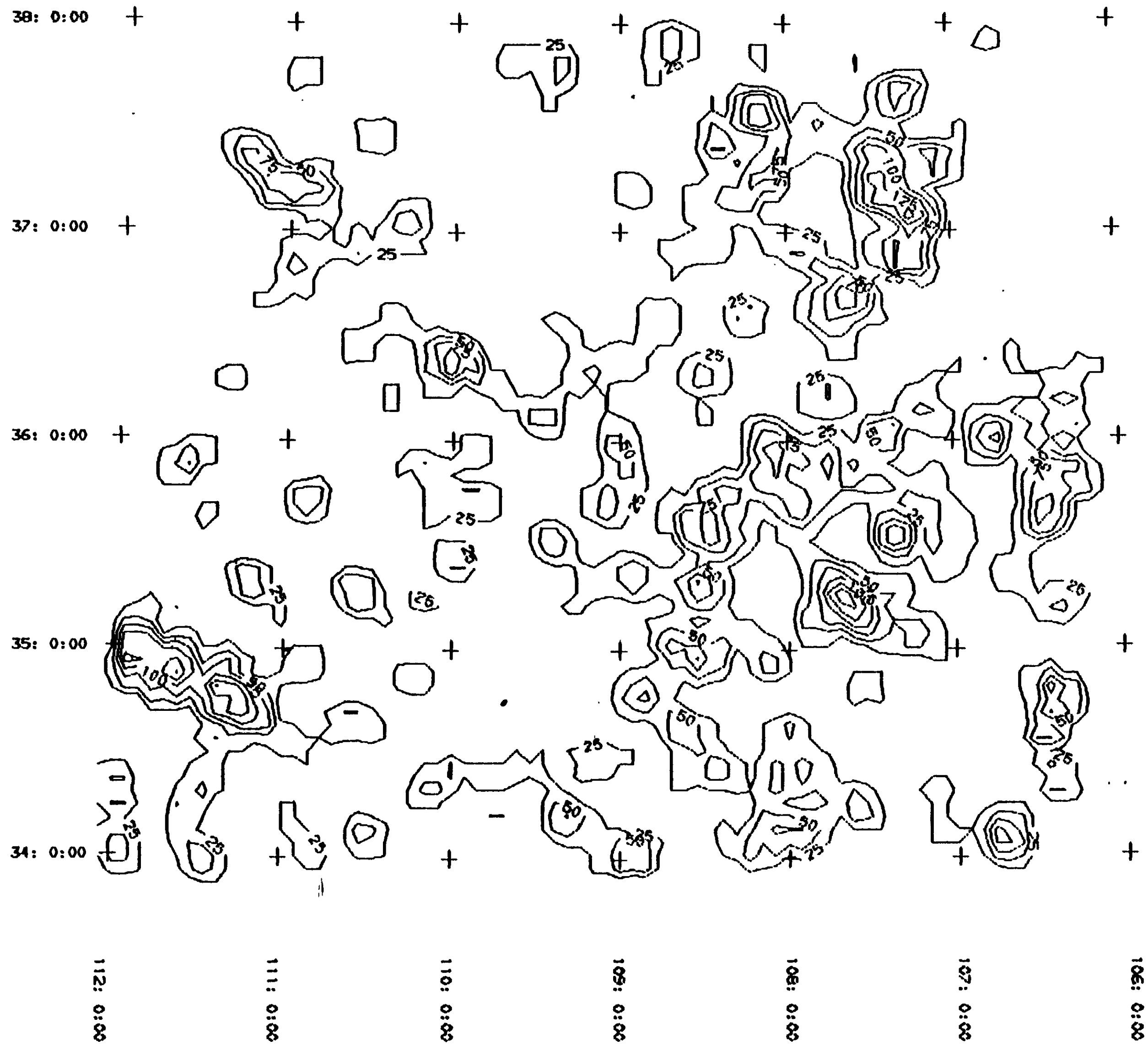

N43-59W I=1; D=7
LINEAR FEATURE CONCENTRATION
CONTOUR INTERVAL = 25

APPENDIX D

Computer-generated Linear Feature and Linear Feature Concnetrations Maps of the Important Azimuthal Trend Intervals Used in This Study, Showing the Interpretation of Derivative Lineaments

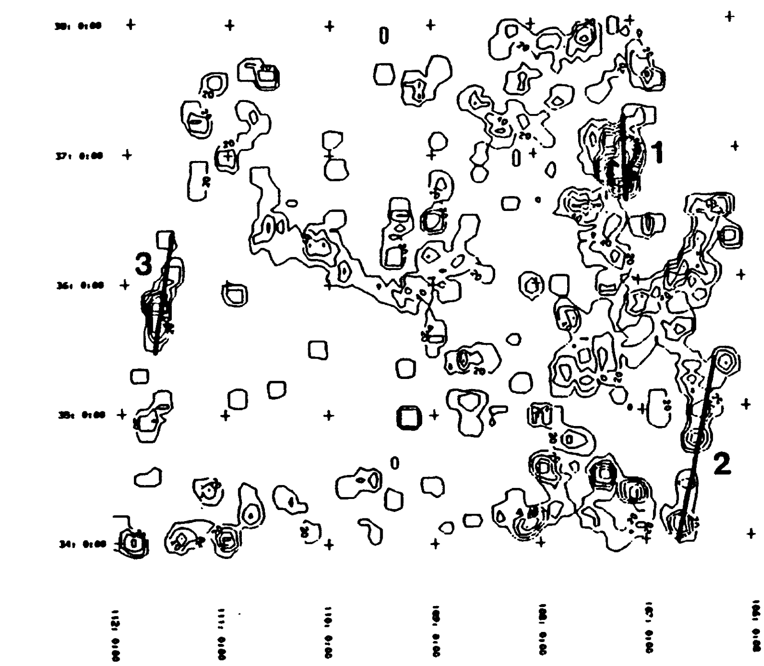

NO-16E I=1; D=6
LINEAR FEATURE CONCENTRATION
CONTOUR INTERVAL= 20

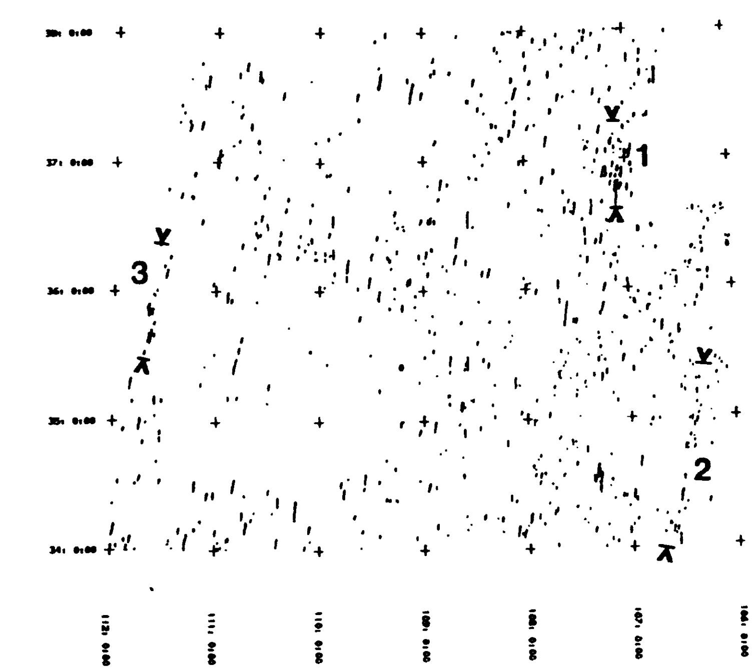

NO-16E LINEAR FEATURES
FOUR CORNERS REGION

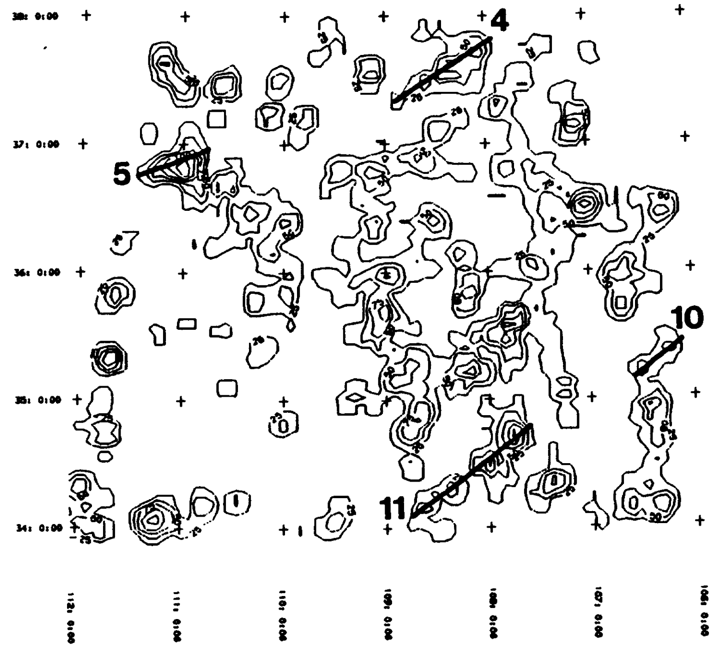

N58-72E 1=1, 0=7
LINEAR FEATURE CONCENTRATION
CONTOUR INTERVAL=25

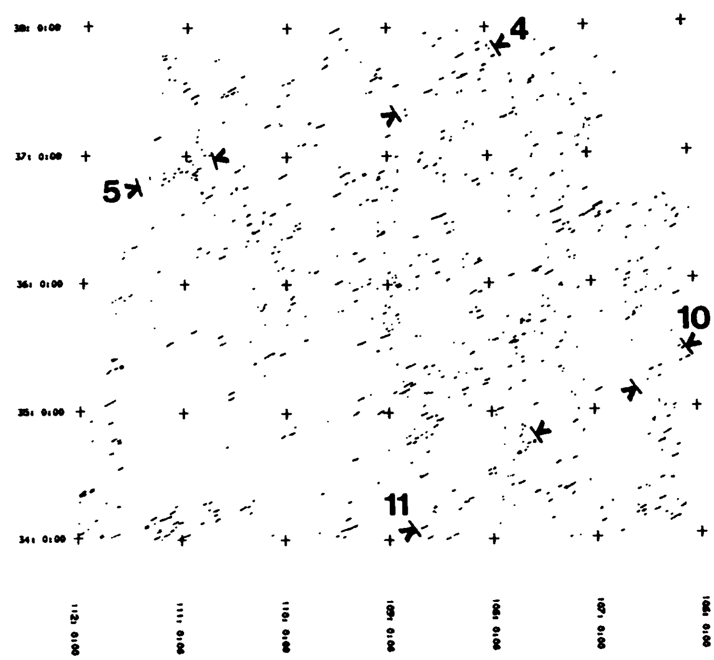

N58-72E LINEAR FEATURES
FOUR CORNERS REGION

N33-43W I=1; D=7
LINEAR FEATURE CONCENTRATION
CONTOUR INTERVAL = 30

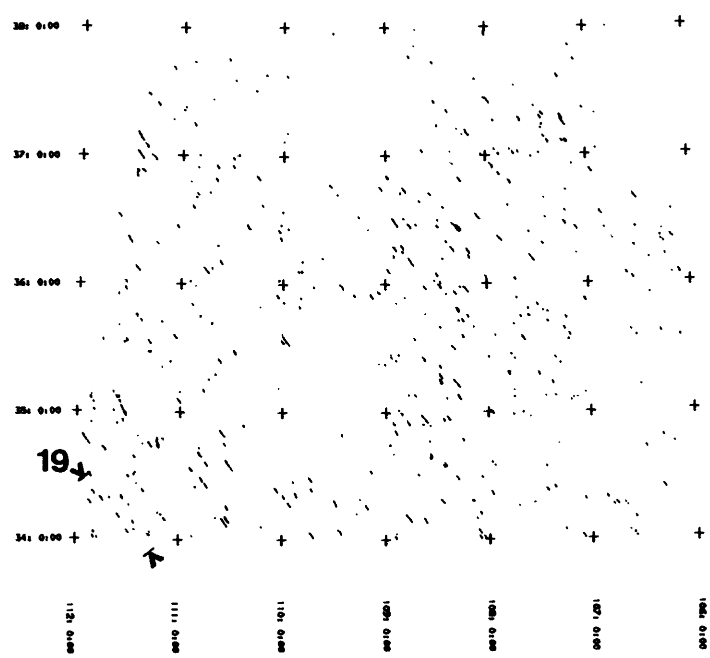

N33-43W LINEAR FEATURES
FOUR CORNERS REGION

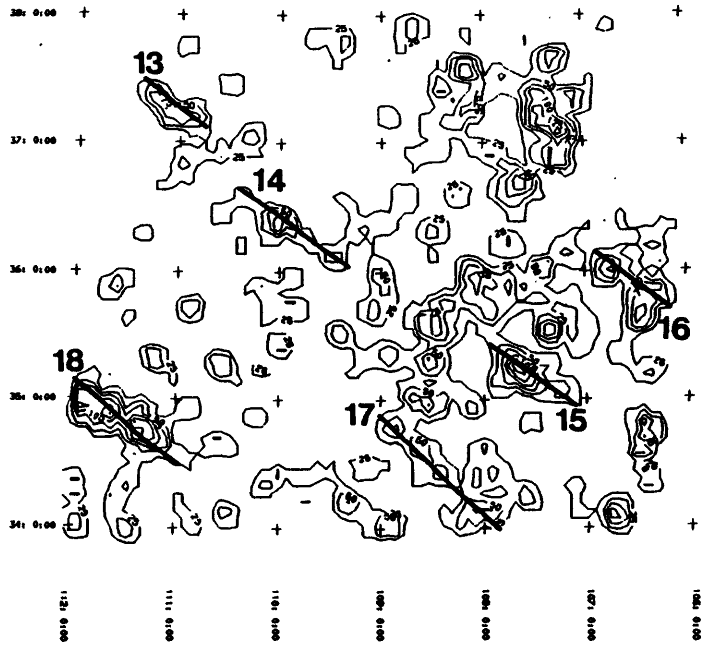

N43-59W 1=1; 0=7
LINEAR FEATURE CONCENTRATION
CONTOUR INTERVAL = 25

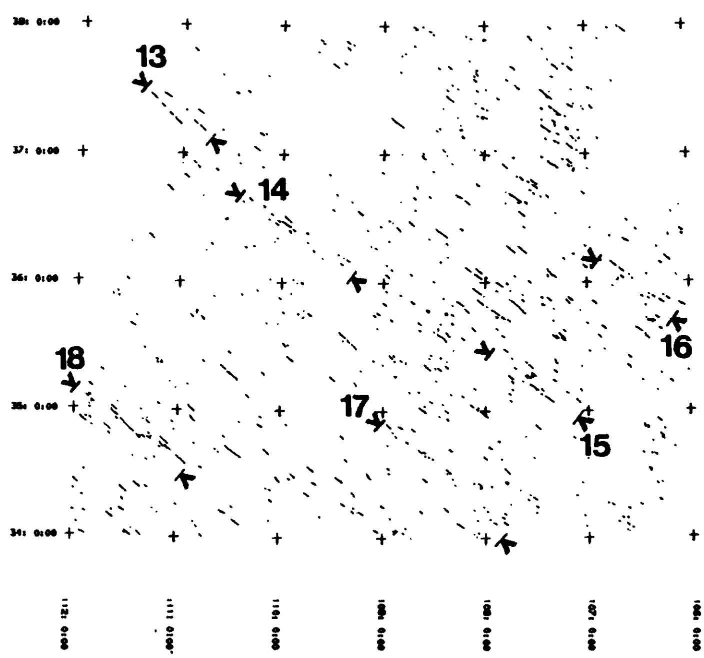

N43-59W LINEAR FEATURES
FOUR CORNERS REGION